


Article

Photoluminescence of Ni(II), Pd(II), and Pt(II) Complexes [M(Me₂dpb)Cl] Obtained from C-H Activation of 1,5-Di(2-pyridyl)-2,4-dimethylbenzene (Me₂dpbH)

Lukas Kletsch ¹, Rose Jordan ¹, Alicia S. Köcher ¹, Stefan Buss ^{2,3}, Cristian A. Strassert ^{2,3,*} and Axel Klein ^{1,*}

- ¹ Department für Chemie, Institut für Anorganische Chemie, Universität zu Köln, Greinstraße 6, D-50939 Köln, Germany; lukas.kletsch@uni-koeln.de (L.K.); rjordan@smail.uni-koeln.de (R.J.); akoecher@smail.uni-koeln.de (A.S.K.)
- ² Institut für Anorganische und Analytische Chemie, Westfälische Wilhelms-Universität Münster, Corrensstr. 28/30, D-48149 Münster, Germany; s_buss14@uni-muenster.de
- ³ CeNTech, CiMIC, SoN, Westfälische Wilhelms-Universität Münster, Heisenbergstr. 11, D-48149 Münster, Germany
- * Correspondence: cstra_01@uni-muenster.de (C.A.S.); axel.klein@uni-koeln.de (A.K.); Tel.: +49-221-470-4006 (A.K.)



Citation: Kletsch, L.; Jordan, R.; Köcher, A.S.; Buss, S.; Strassert, C.A.; Klein, A. Photoluminescence of Ni(II), Pd(II), and Pt(II) Complexes [M(Me₂dpb)Cl] Obtained from C-H Activation of 1,5-Di(2-pyridyl)-2,4-dimethylbenzene (Me₂dpbH). *Molecules* **2021**, *26*, 5051. <https://doi.org/10.3390/molecules26165051>

Academic Editors: Ulrich S. Schubert, Andreas Winter and Athanasios C. Tzipis

Received: 21 July 2021

Accepted: 17 August 2021

Published: 20 August 2021

Publisher's Note: MDPI stays neutral with regard to jurisdictional claims in published maps and institutional affiliations.



Copyright: © 2021 by the authors. Licensee MDPI, Basel, Switzerland. This article is an open access article distributed under the terms and conditions of the Creative Commons Attribution (CC BY) license (<https://creativecommons.org/licenses/by/4.0/>).

Abstract: The three complexes [M(Me₂dpb)Cl] (M = Ni, Pd, Pt) containing the tridentate *N,C,N*-cyclometalating 3,5-dimethyl-1,5-dipyridyl-phenide ligand (Me₂dpb[−]) were synthesised using a base-assisted C-H activation method. Oxidation potentials from cyclic voltammetry increased along the series Pt < Ni < Pd from 0.15 to 0.74 V. DFT calculations confirmed the essentially ligand-centred π*[−]-type character of the lowest unoccupied molecular orbital (LUMO) for all three complexes in agreement with the invariant reduction processes. For the highest occupied molecular orbitals (HOMO), contributions from metal d_{yz}, phenyl C₄, C₂, C₁, and C₆, and Cl p_z orbitals were found. As expected, the d_z² (HOMO-1 for Ni) is stabilised for the Pd and Pt derivatives, while the antibonding d_x²−y² orbital is de-stabilised for Pt and Pd compared with Ni. The long-wavelength UV-vis absorption band energies increase along the series Ni < Pt < Pd. The lowest-energy TD-DFT-calculated state for the Ni complex has a pronounced d_z²-type contribution to the overall metal-to-ligand charge transfer (MLCT) character. For Pt and Pd, the d_z² orbital is energetically not available and a strongly mixed Cl-to-π*/phenyl-to-π*/M(d_{yz})-to-π* (XLCT/ILCT/MLCT) character is found. The complex [Pd(Me₂dpb)Cl] showed a structured emission band in a frozen glassy matrix at 77 K, peaking at 468 nm with a quantum yield of almost unity as observed for the previously reported Pt derivative. No emission was observed from the Ni complex at 77 or 298 K. The TD-DFT-calculated states using the TPSSh functional were in excellent agreement with the observed absorption energies and also clearly assessed the nature of the so-called “dark”, i.e., d-d*, excited configurations to lie low for the Ni complex (≥3.18 eV), promoting rapid radiationless relaxation. For the Pd(II) and Pt(II) derivatives, the “dark” states are markedly higher in energy with ≥4.41 eV (Pd) and ≥4.86 eV (Pt), which is in perfect agreement with the similar photophysical behaviour of the two complexes at low temperatures.

Keywords: nickel; palladium; platinum; cyclometalation; C-H activation; photoluminescence

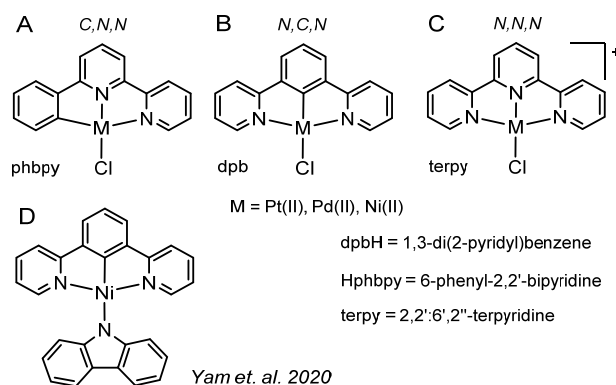
1. Introduction

Luminescent transition metal complexes have gained enormous importance in the last 20 years with potential applications in fields such as photocatalysis [1,2], sensing [3–6], and optoelectronic devices [5–14]. Phosphorescent metal complexes are of particular interest in the field of OLED (organic light emitting diode) applications, as these materials are able to harvest all generated excitons in the operating electroluminescent devices [11]. Efficient intersystem crossing (ISC) and otherwise spin-forbidden phosphorescence is favoured

through large spin-orbit coupling (SOC) of the heavy metal centres [5–11]. Typical phosphorescent emitters are based on metal cations such as the d^6 -configured Re(I), Ru(II), Os(II), and Ir(III) centres [3,4,8–12], or the d^8 -configured Pt(II) or Au(III) species [3–7,9–16]. The d^8 electron configured metals adopt square-planar geometries with open coordination vacancies in the axial positions. These axial flanks can lead to metal–metal ($M\cdots M$) and/or $\pi\cdots\pi$ stacking interactions in aggregates with red-shifted emissions from MMLCT states (metal–metal-to-ligand charge transfer character, eventually with excimeric $M\cdots M$ shortening), along with metal-perturbed ligand-centred ($\pi\text{-}\pi^*$) excited configurations of the monomeric species [17–26].

While phosphorescent Pt(II) complexes are common in the literature, luminescent materials based on the lighter group 10 metals, namely Pd(II) [13,23–32] and Ni(II), [33] are much more scarce. This is attributed to the less efficient SOC associated with the lighter metal ion, as well as to the lower ligand field splitting of the metal d-orbitals providing thermally accessible metal-centred (MC or $d\text{-}d^*$) states with dissociative character, which enable an efficient non-radiative decay pathway back to the ground state via conical intersections [31,34–36].

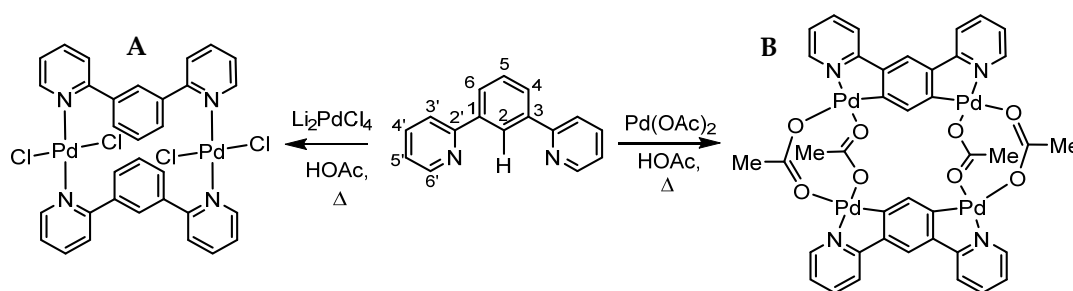
Cyclometalating tridentate or tetradentate ligands revealed to be very suitable to provide a stronger ligand field and move up the so-called “dark” (non-radiative) $d\text{-}d^*$ states in energy above the triplet-emitting metal-to-ligand charge transfer (MLCT) or $\pi\text{-}\pi^*$ states (or mixtures thereof) [5–7,13,16,17,26–30,32,33,37–44]. Amongst them, tridentate C,N,N or N,C,N coordinating units (Scheme 1A,B) derived from the prototypical tridentate N,N,N -ligand 2,2':6',2''-terpyridine (Scheme 1C) constitute a well-studied group [5,7,30,32,33,36–38,42–44]. Their relatively straightforward syntheses and modification by substitution combined with the benefit of a fourth highly variable ancillary ligand at the metal centre makes complexes with these ligands interesting candidates for larger-scale studies. Very recently, a benchmarking study reported on the Ni(II) complex [Ni(dpb)(carbazolate)] (dpbH = 1,3-di(2-pyridyl)benzene (Scheme 1D) which showed triplet emission at 77 K in frozen glassy matrices and at 298 K in the solid state [33].



Scheme 1. Neutral Pt(II), Pd(II), and Ni(II) complexes with cyclometalating C,N,N (A) and N,C,N (B) coordinating ligands phbpy and dpb compared with the analogous cationic complexes with the N,N,N coordinating terpy (C). [Ni(dpb)(carbazolate)] (D) showed triplet emission at 77 K in frozen glassy matrices and at 298 K in the solid state [33].

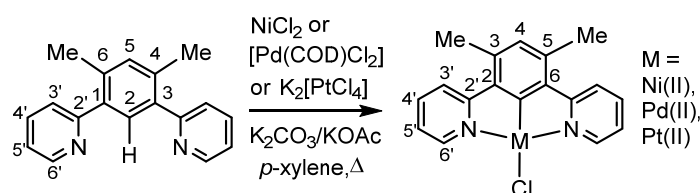
Being interested in comparative studies of isoleptic Pt(II), Pd(II), and Ni(II) complexes [30,32,45,46], we started to explore the three complexes bearing the dpb ligand. Very recently, we found an elegant way to cyclonickelate the dpb ligand forming [Ni(dpb)Cl] [47]. This complex, the precursor for the benchmarking [Ni(dpb)(carbazolate)], was so far only accessible through a transmetalation procedure using the organomercurial [Hg(dpb)Cl] and NiCl₂ [33]. We recently synthesised this key complex in 76% yield using anhydrous NiCl₂ and dpbH in a base-assisted direct metalation in refluxing xylene using the base combination K₂CO₃/KOAc. This reaction was initially developed for the C,N,N coordinating ligand 6-phenyl-2,2'-bipyridine (Hphbpy; Scheme 1A) [48].

Compared with the Ni derivative, the Pt(II) complex [Pt(dpb)Cl] is easily accessible via the established electrophilic C-H activation of the protoligand dpbH with $K_2[PtCl_4]$ in boiling glacial acetic acid (HOAc) and yields of 50 to 80% were reported [38,49–54]. For the Pd derivative [Pd(dpb)Cl], the same method using $Li_2[PdCl_4]$ led to the non-cyclometalated binuclear complex $[Pd_2Cl_2(\mu-\kappa^2N,NdpbH)]$ (Scheme 2A), whereas the use of $Pd(OAc)_2$ gave the cyclometalated tetranuclear $[Pd_4(\mu-\kappa^2, \kappa^2dpb)_2(\mu-\kappa^1, \kappa^1-OAc)_4]$ species (Scheme 2B) [49]. Based on these early findings, the above mentioned transmetalation procedure using [Hg(dpbCl)] was used in a later study [55]. The Hg-transmetalation method was initially developed for the C,N,N coordinated derivative [Pd(phbpy)Cl] [56]. Later, the same authors reported the synthesis of [Pd(dpb)Cl] and a chiral derivative from $Na_2[PdCl_4]$ and dpbH in refluxing HOAc with an 87% yield [51]. However, a successful repetition of this procedure was never reported, although the complex [Pd(dpb)Cl] and its derivatives have been described as promising candidates for Pd-based triplet luminescence or sensitisation [35,36]. In a very recent report, the 6'-(4-OMe)Ph-substituted derivative [Pd(MeOPh₂dpb)Cl] was synthesised from $K_2[PdCl_4]$ and the protoligand in $NaHCO_3$ HOAc/H₂O showed a 42% yield, whereas for the derivative, in which the two methoxy groups were replaced by an intramolecular ether-connection, a 66% yield was achieved [57].



Scheme 2. Cyclometalation reaction of dpbH with $Li_2[PdCl_4]$ (A) and $Pd(OAc)_2$ (B). Adopted from Cardenas, D.J.; Echavarren, A.M.; and Ramirez de Arellano, M.C. in Divergent Behavior of Palladium(II) and Platinum(II) in the Metalation of 1,3-Di(2-pyridyl)benzene, *Organometallics* 1999, 18, 3337–3341, Reference [49].

When trying to apply the base-assisted direct cyclometalation of dpbH with Pd(II) precursors such as $K_2[PdCl_4]$, $PdCl_2$, or $[Pd(COD)Cl_2]$ (COD = 1,5-cyclooctadiene), we were not able to obtain the complex [Pd(dpb)Cl]. Instead, we obtained mixtures of the binuclear and tetranuclear complexes A and B (Scheme 2) together with traces of the target complex and further unidentifiable by-products. In view of the “wrong” cyclometalation site at the 4,6-positions of the dpbH ligand, as shown in the structure F, we decided to use the 4,6-dimethylated dpbH derivative Me_2dpbH (Scheme 3).



Scheme 3. Synthesis of the target $[M(Me_2dpb)Cl]$ complexes from the present study; note the different numbering of the Me_2dpbH protoligand and complexes.

Thus, for the herein reported study, we used the Me_2dpbH protoligand and present the syntheses and characterisation of the three cyclometalated Ni(II), Pd(II), and Pt(II) complexes $[M(Me_2dpb)Cl]$ (Scheme 3) containing the tridentate anionic 3,5-dimethyl-2,6-dipyridylphenide ligand (Me_2dpb^-). The complexes were synthesised using a base-assisted C-H activation method starting from the protoligand 1,3-di(2-pyridyl)-4,6-dimethylbenzene (Me_2dpbH), the suitable metal precursors, and a 1:1 mixture of KOAc and K_2CO_3 in vigorously dried

aprotic solvents. This allowed to study the homologous Ni, Pd, and Pt series of these complexes concerning their fundamental electronic properties through electrochemical methods, UV-vis absorption, and time-resolved photoluminescence spectroscopy, which were interpreted with the aid of (TD-)DFT calculations.

Furthermore, our study allowed us to trace the influence of the two methyl groups of the dpb ligand system. Starting from the parent [Pt(dpb)Cl] systems, various substituents on both ligand parts have been introduced previously and the effects on UV-vis absorption, photoluminescence, and electrochemical potentials were studied [5,16,38,52,54,58–65]. Within this series, [Pt(Me₂dpb)Cl] was very recently synthesised from the protoligand Me₂dpbH and K₂[PtCl₄] in a 50% yield using the “classical” procedure of heating in glacial acetic acid [60]. The electrochemical and photophysical properties of this complex were compared with the un-substituted complex [Pt(dpb)Cl] (dpbH = 1,3-di(2-pyridyl)-benzene) and 1,2,3-triazole-containing derivatives [60]. Thus, the present study also completes the opto-electronic dataset for this complex.

2. Results and Discussion

2.1. Preparation and Analytical Characterisation

The three complexes [M(Me₂dpb)Cl] were synthesised from the protoligand 1,5-di(2-pyridyl)-2,4-dimethylbenzene (Me₂dpbH), anhydrous NiCl₂, [Pd(COD)Cl₂], or K₂[PtCl₄] by using the base-assisted C-H activation method with KOAc and K₂CO₃ in vigorously dried aprotic solvents, as previously reported for the Ni(II) complex [Ni(dpb)Cl] (dpbH = 1,3-di(2-pyridyl)-benzene) [47] and the C,N,N coordinated derivative [Ni(phbpy)Cl] (Hphbpy = 6-phenyl-2,2'-bipyridine) [48]. The three products were characterised through elemental analyses, EI-MS(+), ¹H, and ¹³C NMR spectroscopy, and additionally ¹⁹⁵Pt NMR for [Pt(Me₂dpb)Cl] (see Supplementary Materials). The ¹H and ¹³C NMR of the Pt(II) complex matched perfectly the previously reported data [60].

The Pt derivative [Pt(Me₂dpb)Cl] was previously synthesised via the classical method of heating the ligand and K₂[PtCl₄] in glacial acetic acid [38,50,52–54] for about 1 h with a yield of 50% [60]. With a 70% yield, our method is superior, while the reaction time was markedly longer.

Using the base-assisted C-H activation method with KOAc and K₂CO₃ in *p*-xylene, the yield for the Pd derivative was increased from 6% to 68% by avoiding light. Importantly, this procedure replaces the previously applied transmetalation using organomercurials [55] and we are optimistic to be able to increase the yield even more through optimisation of the reaction conditions. When applying the same procedure for the unsubstituted protoligand dpbH with Pd, we obtained the aforementioned and previously reported tetrameric complex [Pd₄(μ-κ²,κ²-dpb)₂(μ-κ¹,κ¹-OAc)₄] with yields of up to 31% [49]. When using pivalic acid (HOPiv) instead of HOAc, we obtained the complex [Pd₄(μ-κ²,κ²-dpb)₂(μ-κ¹,κ¹-OPiv)₄] with a 28% yield (see Experimental Section and Supplementary Materials, Scheme S1). Then, we explored the synthesis of [Pd(Me₂dpb)Cl] through reaction of the ligand with Na₂[PdCl₄] in acetic acid, as reported for the unsubstituted derivative [Pd(dpb)Cl] (87%) [52], and obtained the target complex in a 98% yield.

The yield of 94% for the Ni complex [Ni(Me₂dpb)Cl] is excellent and markedly exceeded the yield for the unsubstituted derivative [Ni(dpb)Cl], reaching 76% [47].

To summarise the synthesis experiments, the base-assisted metalation works for all three elements but with very different yields of 94% for Ni and about 70% for Pt and Pd. While for Ni our method is without an alternative, the yields for the Pt complex were comparable to those of other methods. For the Pd complex, the classical electrophilic substitution—i.e. heating the components in acetic acid—gave an excellent yield of 98%, which so far exceeds our base-assisted metalation method.

2.2. X-ray Diffractometric Analysis of Single Crystals and DFT-Calculated Structures

From the Pt, Pd, and Ni complexes, single crystals were obtained for X-ray diffraction experiments. For Ni, the compound [Ni(Me₂dpb)Cl]·CH₂Cl₂ was solved and refined in

an orthorhombic cell in the space group *Pbca* (Table S1, Figures S1–S3). Unfortunately, the overall quality of this structure is low, which is due to the poor characteristics of the crystals ($R_{\text{int}} \sim 24\%$). The molecular metrics were refined to reasonable values and the agreement with the DFT-calculated data was good (Table S2). $[\text{Pd}(\text{Me}_2\text{dpb})\text{Cl}]$ crystallised without solvent molecules and the structure was solved in monoclinic *P21/c* with excellent refinement parameters (Table S1, Figures S4–S6). For Pt, we obtained the previously reported triclinic structure (*P-1*) for the compound $[\text{Pt}(\text{Me}_2\text{dpb})\text{Cl}] \cdot \text{CH}_2\text{Cl}_2$ [60].

The experimental data for the Pd complex $[\text{Pd}(\text{Me}_2\text{dpb})\text{Cl}]$ and the previously reported data for the Pt complex $[\text{Pt}(\text{Me}_2\text{dpb})\text{Cl}] \cdot \text{CH}_2\text{Cl}_2$ were used to benchmark our DFT geometry-optimisation (BP86/def-TZVP/D3/COSMO(THF)) on the reported data (Figure 1) with a very good agreement between the calculated molecular metrics and reported values (Tables S3 and S4).

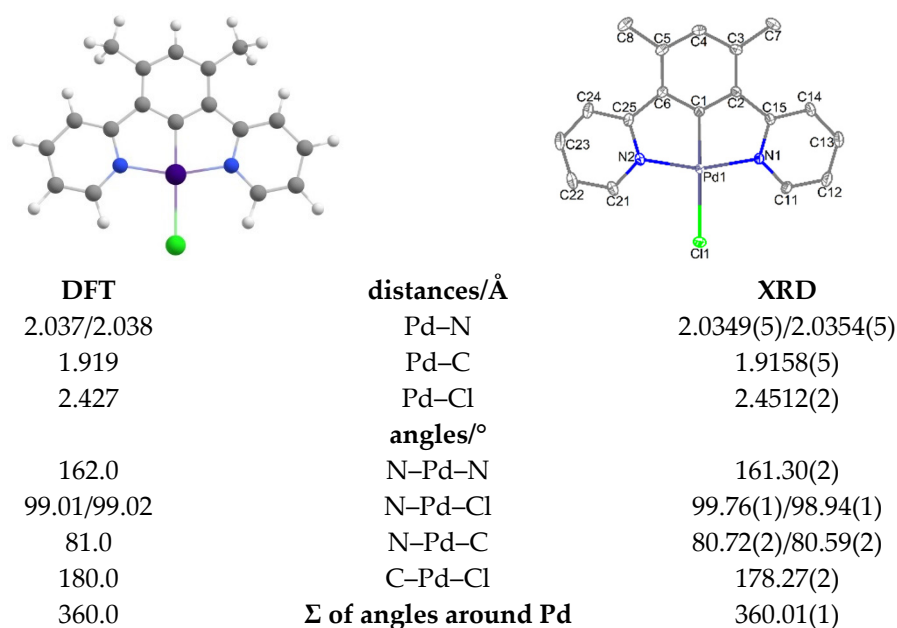


Figure 1. DFT-calculated molecular structure of $[\text{Pd}(\text{Me}_2\text{dpb})\text{Cl}]$ (left) and experimental structure from single crystal X-ray diffraction (ORTEP plot with displacement ellipsoids at 50% probability, right) (Table S3).

2.3. Electrochemistry and DFT Calculations of Frontier Orbitals

At first glance, the electrochemical behaviour of the three complexes $[\text{M}(\text{Me}_2\text{dpb})\text{Cl}]$ is very different. The cyclic voltammograms (CVs) of the Pt and Pd complexes exhibit reversible first reduction processes and for the Pt derivative, even a second reversible process is found (Figure 2). For the Ni derivative, a completely irreversible first reduction is followed by a partially reversible second process and a third irreversible wave. The same features were found for the unsubstituted Ni complex $[\text{Ni}(\text{dpb})\text{Cl}]$ and ascribed to rapid cleavage of the halide Cl^- after reduction [47]. Such an EC (electrochemical reduction + chemical reaction) mechanism was previously studied in detail for the *C,N,N* coordinated complex $[\text{Ni}(\text{phbpy})\text{Br}]$ [66,67]. The reversible behaviour of the Pd and Pt complexes $[\text{M}(\text{Me}_2\text{dpb})\text{Cl}]$ means that the Cl^- cleavage is not observed on the timescale of the CV experiment. A reversible behaviour was also previously reported for derivatives of $[\text{Pt}(\text{Rdpb})\text{Cl}]$ (HRdpy = substituted 1,5-di(2-pyridyl)-benzene) [50,60]. The two observed reduction potentials for the Pt and Pd complex differ by quite constant values (0.41 and 0.45 V; ΔE (Red1-Red2), Table 1), which stands in contrast to the *C,N,N* coordinated complexes $[\text{M}(\text{phbpy})\text{Cl}]$, for which the separation is markedly larger (~ 0.68 V). This and the overall lower reduction potentials is in agreement with the superior accepting properties of the phbpy ligand that contains a 2,2'-bipyridine unit, in contrast to the two

phenyl-separated pyridyl units of the dpb ligand [47], and is a clear indication of dpb-based reduction processes for all three complexes. In addition, for the oxidation processes, the Ni derivative (reversible wave) differs markedly from the Pt and Pd (both irreversible) species.

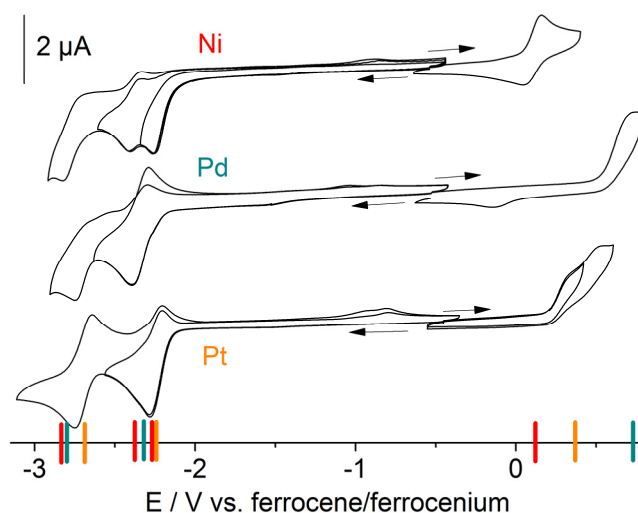


Figure 2. Cyclic voltammograms of $[M(\text{Me}_2\text{dpb})\text{Cl}]$ in $n\text{-Bu}_4\text{NPF}_6/\text{THF}$. Coloured bars represent half-wave potentials ($E_{1/2}$) for reversible reductions and anodic peak potentials (E_{pa}) for irreversible oxidations.

The first reduction potentials at around -2.3 V are similar for all three complexes with only slightly lower values for the Pd derivative (Table 1). In contrast to this, the oxidation processes are very different for the three metals following the series $\text{Ni} < \text{Pt} < \text{Pd}$. In recent studies on such homologous series including the series $[M(\text{phbpy})(\text{X})]$ ($\text{X} = \text{Cl}$ or CN), the oxidation potentials increased along the series $\text{Ni} < \text{Pt} < \text{Pd}$ [32,46]. However, ultraviolet photoelectron spectroscopy (UPS) on a series of the three metals chelated with an O,N,N,S -coordinating phenolate-pyridine thiosemicarbazone, the observed ionisation energy ranked as $\text{Pt} < \text{Ni} < \text{Pd}$ [46].

DFT-based single point calculations were performed on the optimised geometries using the hybrid functional TPSSH [68], which has recently been shown to provide qualitatively very good results for organometallic Ni and also for Pd and Pt complexes [46,47,69]. The calculations show an essentially ligand-centred π^* -type lowest unoccupied molecular orbital (LUMO) with very similar energies for all three complexes at around -2.3 eV (Figure S8), in agreement with the invariant experimental reduction potentials (Figure 2). The largest contribution comes from the two pyridyl units, while C1, C2, and C6 from the central phenyl core have only a minor impact. For the second LUMO (i.e., LUMO+1), the phenyl C2, C3, C5, and C6 show marked contributions. This is in line with rather invariant reduction potentials of the Pt(II) complexes of substituted dpb ligands (Table 1). 3,5-Me₂-substitution leads to slightly lower (more negative) potentials, while 4-Me substitution has no impact [50,54]. Slightly higher (less negative) reduction potentials were obtained for F- or CF₃-substituted derivatives (Table 1) with the highest reported shift of $+0.26$ V compared with the parent Pt complex when introducing the 3,5-(CF₃)₂-dpb ligand [54]. Metal contributions of the $d_x^2-y^2$ -type orbital to the unoccupied MOs are found lowest in energy for Ni (LUMO+3) and markedly higher for both Pd (LUMO+4) and Pt (LUMO+5), as expected from the drastically increased ligand field across the series $\text{Ni} < \text{Pd} < \text{Pt}$.

Table 1. Redox potentials of Me₂dpbH, of complexes [M(Me₂dpb)Cl] (M = Pt, Pd, Ni), and of comparable complexes ^a.

	<i>E</i> _{pc} (Red2)	<i>E</i> _{1/2} (Red1)	<i>E</i> _{pa} (ox1)	ΔE (Red1-Red2)	ΔE (ox1-Red1)	Solvent	DFT ^k
Me ₂ dpbH	−2.52	−1.74 irr	-	0.70	-	THF	
[Ni(Me ₂ dpb)Cl]	−2.37 rev ^b	−2.26 irr	0.10 rev	0.11 (0.45) ^b	2.36	THF	3.07
[Pd(Me ₂ dpb)Cl]	−2.75	−2.34	0.74	0.41	3.07	THF	3.39
[Pt(Me ₂ dpb)Cl]	−2.69	−2.24	0.35 ^c	0.45	2.59	THF	3.15
[Pt(dpb)Cl] ^d	-	−2.14	0.35	-	2.49	MeCN	
[Pt(4-Medpb)Cl] ^d	-	−2.15	0.29	-	2.44	MeCN	
[Pt(4-MeOOCdpb)Cl] ^d	-	−2.04	0.39	-	2.43	MeCN	
[Pt(dpb)Cl] ^e	-	−2.18	0.41	-	2.59	DMF	
[Pt(3,5-(CF ₃) ₂ dpb)Cl] ^e	-	−1.92	0.50	-	2.42	DMF	
[Pt(3,4,5-F ₃ dpb)Cl] ^e	-	−2.07	0.51	-	2.58	DMF	
[Pt(Me ₂ dpb)Cl] ^f	-	−2.03	0.43	-	2.46	CH ₂ Cl ₂	
[Ni(dpb)Cl] ^g	−2.57	−2.33 irr	0.06 rev	0.24	2.39	THF	
[Ni(phbpy)Cl] ^{h,i}	−2.60 rev	−1.93	0.06 rev	0.67	1.99	THF	
[Pd(phbpy)Cl] ⁱ	−2.60 rev	−1.92	0.80 ^b	0.68	2.72	THF	3.58
[Pt(phbpy)Cl] ⁱ	−2.48 rev	−1.78	0.41	0.70	2.19	THF	

^a From cyclic voltammetry in *n*-Bu₄NPF₆/THF (tetrahydrofuran). Potentials in V vs. ferrocene/ferrocenium; half-wave potentials (*E*_{1/2}) for reversible processes (rev); cathodic peak potentials (*E*_{pc}) for irreversible reductions (irr); accuracy of potentials: ± 0.003 V. ^b When taking into account the third irreversible reduction at −2.82 V, the separation between the second and third potential fits to the 0.45 V observed for the Pt and Pd derivatives. However, we assume that the [Ni(Me₂dpb)(THF)]⁺ complex causes the second and third reduction processes (see text). ^c Further irreversible oxidation at 0.52 V. ^d From Reference [50]. ^e From Reference [54]. ^f Reduction measured in MeCN and oxidation in CH₂Cl₂ from Reference [60]. ^g From Reference [47]. ^h From Reference [70]. ⁱ From Reference [71]. ^k DFT-calculated HOMO-LUMO gaps for the S₀ states.

The highest occupied molecular orbital (HOMO) gains essential contributions from phenyl C4, C2, C1, and C6, as well as metal d_{yz} and Cl p_z orbitals (the *y*-axis bisects the molecule and *z* stands perpendicular to the coordination plane, Figure S8). Although their character is similar for the three metals, the energies are quite different, decreasing from Ni > Pt > Pd and thus excellently reproducing the series of oxidation potentials, which confirms the versatility of the TPSSh functional for the entire triad [46,47,68,69]. The calculated compositions also agree very well with the observation that the methyl substitution in the 3,5-positions (dpb → Me₂dpb) does not have a marked effect on the oxidation potential, while the 4-methyl or 4-methylester substitution strongly modifies the oxidation potential. An orbital with d_z² character forms the HOMO-1 orbital for Ni; for Pd, an orbital of the d_{xy}-type lies at the same energy; and for Pt, the d_z² orbital is markedly lower in energy than the d_{xy}-type, again properly reproducing the trends in ligand field splitting within the triad. These differences might also account for the variations in reversibility for the oxidation. Experimentally, the oxidation potentials are quite invariant upon substitution of the parent [Pt(dpb)Cl] complex, as outlined above, but a marked solvent effect is found (Table 1) in agreement with the oxidation locus extended over the phenyl-M-Cl unit.

The calculated HOMO-LUMO gaps increase along the series Ni < Pt < Pd and thus qualitatively agree well with those derived from the electrochemical measurements (ΔE (ox1-red1) (Table 1).

2.4. UV-Vis Absorption Spectroscopy and TD-DFT Calculated Transitions

The UV-vis absorption spectra of the three complexes in the CH₂Cl₂ solution (Figure 3, data in Table 2) are characterised by very intense bands in the UV-range of up to 300 nm. Since they also occur for the protoligand Me₂dpbH, we can assign them to transitions into π - π^* states. They are followed by intense, structured absorptions in the range of 300 to 450 nm. For the Ni complex, the long-wavelength absorption band shows a maximum at 395 nm, an intense shoulder at 420 nm, a small component at 465 nm, and finally tails down to a cut-off at 516 nm (Figure 3A insert). For the Pt derivative, the maximum of this band is blue-shifted to 380 nm and the cut-off appears at 442 nm. For the Pd complex, the maximum is even more blue-shifted to 360 nm and the cut-off shifts to 402 nm. Thus, there

is a clear series of increasing optical gaps, i.e., Ni (2.40) < Pt (2.80) < Pd (3.08), when taking these cut-off energies into account. They are slightly higher than the electrochemical gaps for Ni (+0.04 eV) and Pd (+0.01 eV), but markedly different for Pt (+0.21 eV). Basically, these differences represent the reorganisation after the oxidation or reduction compared with the vertical Franck–Condon excitation.

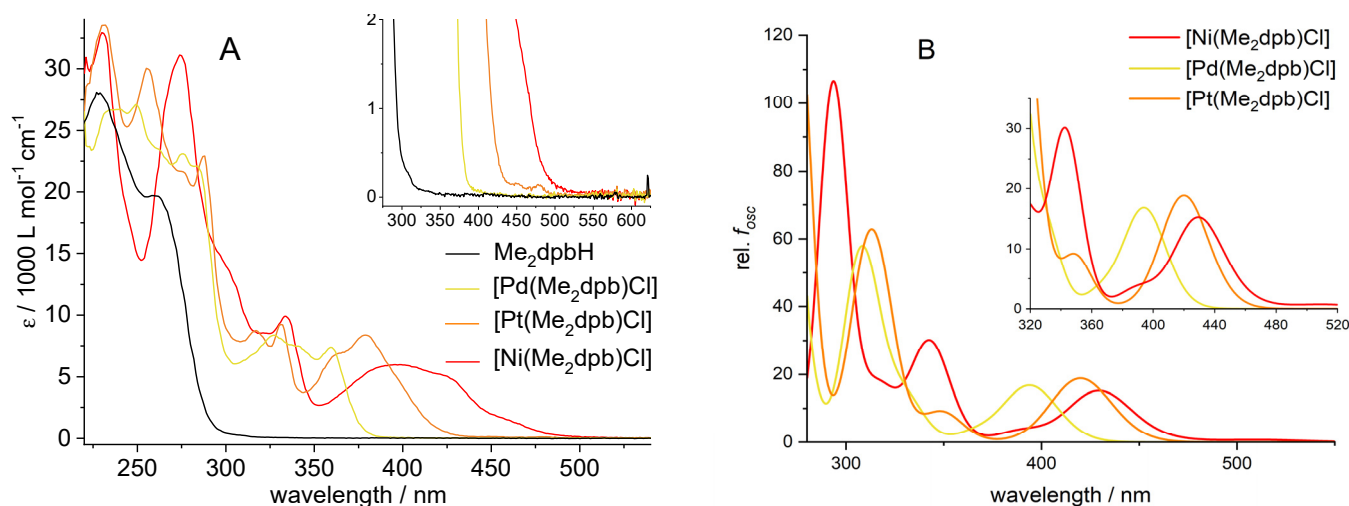


Figure 3. UV-vis absorption spectra of Me₂dpbH and the complexes [M(Me₂dpb)Cl] in CH₂Cl₂ solution (A) and TD-DFT-calculated spectra (B) (TPSSH/def2-TZVP level of theory). The yellow (Pd), orange (Pt), and red (Ni) colour code refer to the colours of the compounds.

Table 2. Selected UV-vis absorption maxima of Me₂dpbH, the complexes [M(Me₂dpb)Cl], and related derivatives ^a.

	λ_1 (ε)	λ_2 (ε)	λ_3 (ε)	λ_4 (ε)	λ_5 (ε)	λ_6 (ε)	λ_7 (ε)
Me ₂ dpbH— <i>this work</i>	227 (28.2)	260 (19.7)	340 (0.4)	636 (0.3)	-	-	-
[Pt(Me ₂ dpb)Cl]— <i>this work</i>	231 (33.7)	256 (30.0)	287 (22.9)	331 (9.2)	380 (8.3)	413 (1.5)	480 (0.1)
[Pd(Me ₂ dpb)Cl]— <i>this work</i>	239 (26.7)	275 (23.2)	283 (22.0)	327 (8.3)	360 (7.4)	375 (1.2)	-
[NiMe ₂ dpb)Cl]— <i>this work</i>	230 (33.0)	274 (31.2)	297 (14.7)	333 (9.0)	395 (6.1) ^b	-	465 (1.1)
[Pt(dpb)Cl] ^{c,e,e,f}	-	255 (25.2)	289 (21.1)	332 (6.3)	379 (8.6)	402 (7.0)	485 (0.1)
[Pt(4-Medpb)Cl] ^d	-	-	-	335 (5.7)	381 (6.9)	412 (6.8)	495 (0.1)
[Pt(4-MeOOCdpb)Cl] ^d	-	-	-	329 (7.5)	380 (9.9)	397 (7.9)	478 (0.2)
[Pt(3-F-dpb)Cl] ^e	-	-	-	-	379 (9.1)	401 (5.2)	477 (0.1)
[Pt(3,5-F ₂ -dpb)Cl] ^e	-	-	-	-	375 (7.6)	-	467 (0.1)
[Pt(3,4,5-F ₃ -dpb)Cl] ^c	-	-	-	-	380 (10.4)	405 (4.6)	480 (0.1)
[Pt(3,5-(CF ₃) ₂ -dpb)Cl] ^c	-	-	-	-	382 (10.4)	408 (8.6)	479 (0.2)
[Ni(dpb)Cl] ^g	236 (35.5)	279 (26.8)	-	332 (5.7)	412 (6.3)	437 (6.7)	-
[Ni(phbpy)Cl] ^{g,h}	281	-	321	354	391	596	-
[Pd(phbpy)Cl] ^{h,i,k}	266 (20)	278 (21)	311 (12)	325 (13)	342 (8)	402 (1)	-
[Pt(phbpy)Cl] ^{h,i}	278	302	330	363	410	430	-

^a Absorption maxima λ in nm in fluid CH₂Cl₂ solution at rt; molar absorption coefficient ϵ in 1000 L mol⁻¹ cm⁻¹. ^b Further shoulder at 420 (5.3). ^c From Reference [54]. ^d From Reference [50]. ^e From Reference [58]. ^f From Reference [72]. ^g From Reference [47]. ^h From Reference [70]. ⁱ From Reference [71]. ^k From Reference [42].

A closer look reveals some low-energy features with very low intensities at 450 and 480 nm for the Pt complex (Figure 3A, insert, and Table 2, λ_7). They are ascribed to the spin-forbidden transitions into the triplet manifold. They partly gain allowance due to the large spin-orbit coupling (SOC) of Pt [11,38,63] and have been previously reported for [Pt(Me₂dpb)Cl] [60] and the complex [Pt(dpb)Cl] with the unsubstituted ligand [50]. The absorption spectra recorded for [Pt(Me₂dpb)Cl] fully agrees with the previously reported data [60].

When comparing Pt complexes with substituted dpb ligands, rather small variations were found for the dominant band maximum at around 380 nm (Table 2, λ_5); e.g., for the

3,5-difluorinated derivative [Pt(3,5-F₂-dpb)Cl], this band is blue-shifted by only 350 cm⁻¹ from 380 nm to 375 nm if compared with the Me₂dpb or dpb complex [58]. However, 3,5-substitution seems to shift the long-wavelength component at around 400 nm (Table 2, λ₆), which is visible for the parent dpb complex, the 4-Me and 4-MeOOC [50] derivatives, and also for the 3-F complex [58] (Table 2). Remarkably, substitution with electronegative groups as in 3,4,5-F or 3,5-CF₃ seems to be detrimental for a blue-shift of the 380 nm band and the absorption maxima of these two complexes lie very close to the parent complex [54].

TD-DFT calculated transitions generally agree qualitatively well with experimentally observed absorption maxima (Figure 4 and Figure S9, Tables S6–S8) with the calculated low-energy transitions at 429 nm (Ni), 420 nm (Pt), and 394 nm (Pd), but slightly red-shifted if compared with the experimental maxima (395, 380, 360 nm). These bands have approximately the same character for the Pt and Pd derivatives and are best described as transitions into Cl(p)-M(d_{yz})-ph to ligand π*(py) charge transfer states with mixed XLCT/MLCT/ILCT character (Figure 4, left). The calculated vertical S₀→S₁ transitions (Tables S6 and S7) show that these bands essentially mirror the excitation into HOMO→LUMO+1 configurations, while the HOMO→LUMO configured states were calculated with energies corresponding to 435 nm for Pt and to 403 nm for Pd but with very low intensities. However, they match very well with the so-called optical cut-offs for these two complexes at 442 nm (Pt) and 402 nm (Pd). Moreover, a look at the calculated frontier orbitals of the ground states shows that an overlap of the HOMO with the LUMO+1 looks more probable than with the LUMO (Figure S8). Both findings strongly support our calculations and assignments.

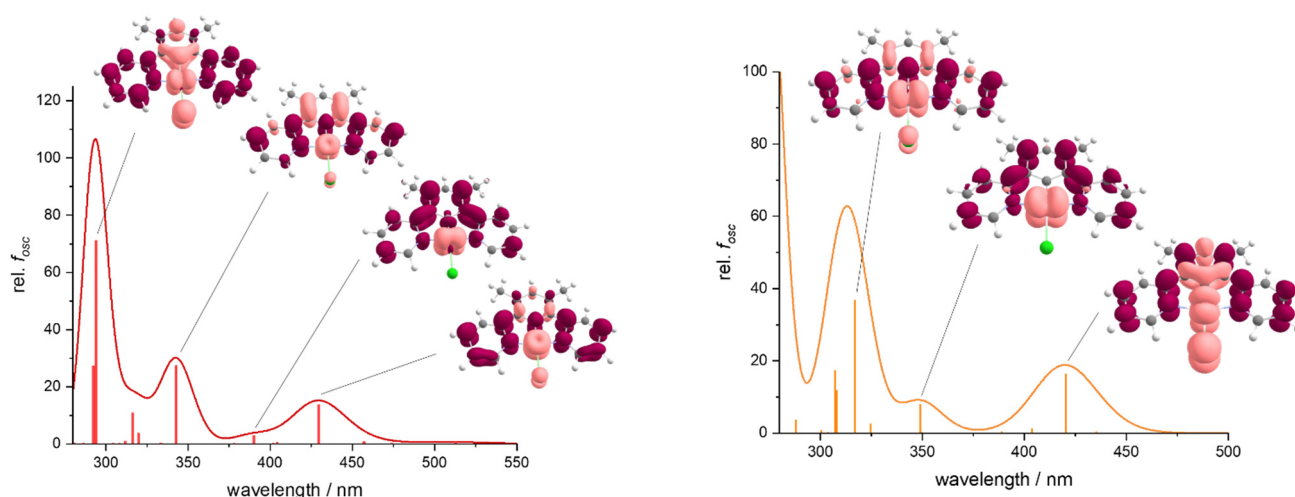


Figure 4. TD-DFT-calculated transitions for [M(Me₂dpb)Cl] with M = Pt (**left**) and Ni (**right**), calculated at the TPSSh/def2-TZVP level of theory.

For the Ni complex, the lowest-energy transition has markedly lower Cl-character and the contributions of the phenyl group are different from those of the Pd and Pt derivatives, and they are also generally smaller (Figure 4). Thus, for the Ni complex, we can relate the long-wavelength transition to an excitation into a state with almost pure MLCT character (d_{z²} to π*). The calculated vertical S₀→S₁ transitions (Table S8) confirm this and show that the 429 nm band corresponds to an S₁ state with almost equal HOMO-2→LUMO (52%) and HOMO→LUMO+1 (43%) contributions. The HOMO-1→LUMO configuration is calculated with an energy of 513 nm and matches perfectly the optical cut-off observed at 516 nm.

The different character of the states involved in the long-wavelength bands for the Ni complex and for the heavier homologues is due to the energetic availability of the Ni d_{z²} orbital, while for the Pd and Pt derivatives, this orbital is markedly stabilised in relation to the calculated energies and composition of the S₀ ground state (Figure S8).

The shoulder calculated at 390 nm for the Ni complex corresponds to a transition into a state with high MLCT (d_{xz} to π^* ; HOMO-1 \rightarrow LUMO+1, 62%) character with the π^* extending over the pyridyl and phenyl cores, but it also obtains a marked contribution from the Ni $d_{x^2-y^2}$ (HOMO-1 \rightarrow LUMO+3 configuration, 16%). For the Pd and Pt derivatives, this kind of transition is blue-shifted to 349 nm for Pt and 331 nm for Pd and does not contain any contribution from $d_{x^2-y^2}$ orbitals to the excited state configuration. For Pd, the lowest energy state with such $d_{x^2-y^2}$ component is reached at 281 nm (HOMO-2 \rightarrow LUMO+4, 71%), while for Pt, a band at 255 nm involves such states (HOMO-2 \rightarrow LUMO+5, 38%). This perfectly reflects the strongly increased ligand field splitting for Pd(II) and Pt(II) compared with Ni(II) and is in line with the efficient photoluminescence for the Pt and Pd complexes, while for Ni, the low-lying excited d-d* configuration very probably quenches the luminescence through radiationless relaxation (see later). In contrast to this, the 343 nm band of the Ni complex is related to a state with mixed ILCT/MLCT character, which is unmatched by Pt and Pd.

The most intense bands in the spectra around 300 nm differ markedly for all three complexes with respect to the excited state character. For the Pt derivative, a mixed ILCT/MLCT contribution was observed with a strong Pt(d_{xz}) component and a rather low Cl(p_z) participation. For the Pd complex, the Cl(p_z) contribution is increased while the participation of the phenyl core is almost vanished, and an overall mixed XLCT/MLCT character must be ascribed (Figure S9). For the Ni derivative, the phenyl contribution becomes strongest within this series and is very similar to the character of the state reached by long-wavelength transitions, where a mixed XLCT, ILCT, and MLCT character is found involving metal d_{xz} contribution.

2.5. Spectroelectrochemistry

Upon electrochemical reduction, all the three complexes $[M(\text{Me}_2\text{dpb})\text{Cl}]$ exhibit long-wavelength absorptions at around 600 and 400 nm (Figure 5, Figures S10 and S11). We ascribe them to the radical anionic complexes $[M(\text{Me}_2\text{dpb})\text{Cl}]^{\bullet-}$ or $[M(\text{Me}_2\text{dpb})(\text{THF})]^\bullet$ when assuming the cleavage of the Cl^- ligand after reduction. The bands can be assigned to transitions into $\pi^*-\pi^*$ states within the reduced dpb ligand frame and they are very similar to those observed for $[\text{Ni}(\text{dpb})\text{Cl}]$ [47]. The subtle red-shift of these two bands upon the second reduction for the Pt complex (Figure 5) confirms this assignment. Upon oxidation, the long-wavelength MLCT bands vanish. As in all three cases, the oxidations are irreversible in the CV experiment and the species produced upon oxidation are not clear. However, in all three cases, very similar spectroscopic features are observed (Table S9) and pointing to comparable products from oxidation and subsequent chemical reaction (decomposition).

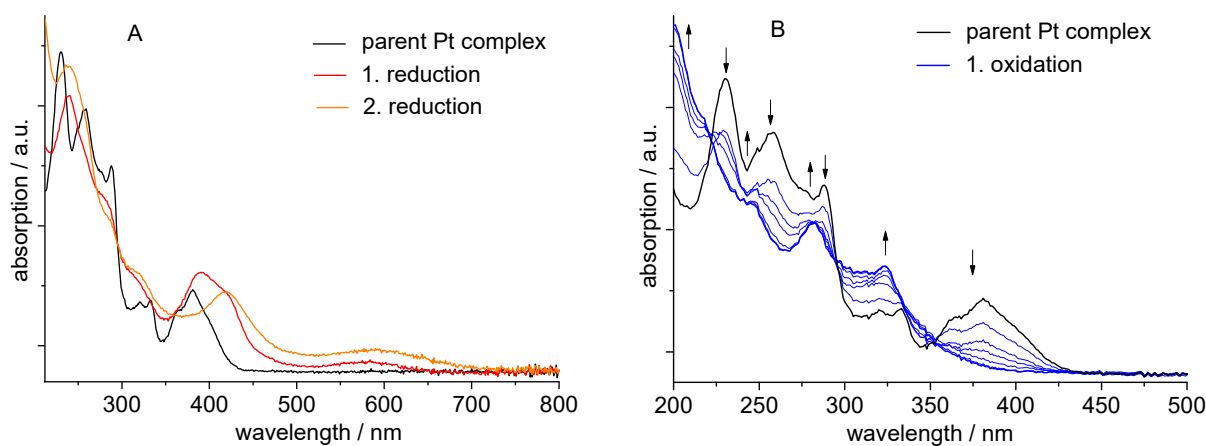


Figure 5. UV-vis absorption spectra of $[\text{Pt}(\text{Me}_2\text{dpb})\text{Cl}]$ in $\text{THF}/n\text{-Bu}_4\text{NPF}_6$, recorded during cathodic reduction (A) and anodic oxidation (B).

2.6. Photoluminescence Spectroscopy

We studied the photoluminescence of the three complexes $[M(\text{Me}_2\text{dpb})\text{Cl}]$ ($M = \text{Pt}$, Pd , and Ni) alongside with the unsubstituted $[\text{Pt}(\text{dpb})\text{Cl}]$ at 298 K in fluid solutions (DCM and 2-MeTHF) and at 77 K in frozen glassy 2-MeTHF matrices. Under none of these conditions did the Ni complex show any photoluminescence (PL), which is consistent with the relatively low-lying d-d* states calculated for Ni (390 nm or 3.18 eV) compared with Pd (281 nm or 4.41 eV) and Pt (255 nm or 4.86 eV). The photophysical properties are summarised in Figure 6 and Table 3, and the full set of spectra and photoluminescence decays is shown in Figures S12–S25.

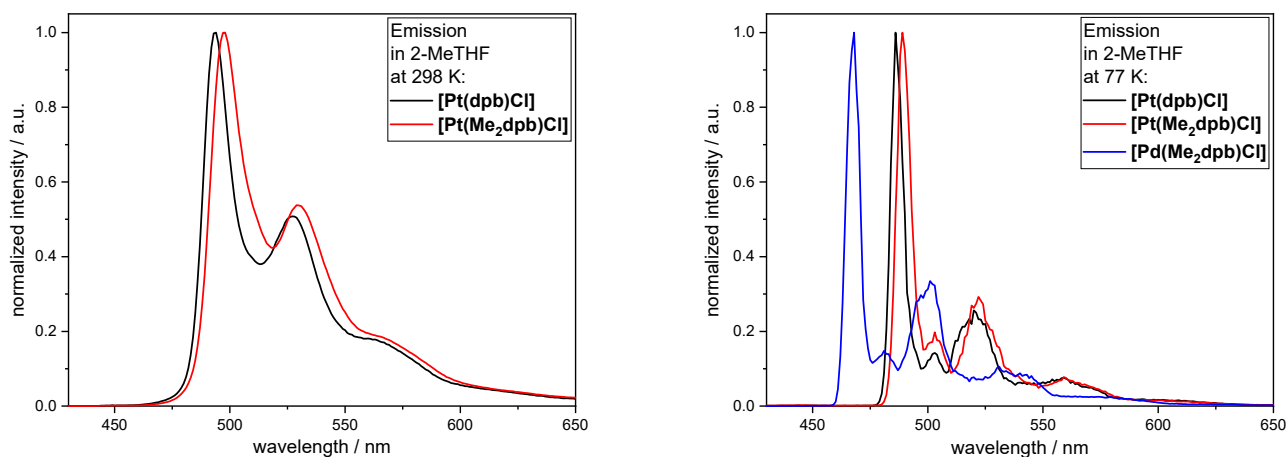


Figure 6. Photoluminescence spectra of $[\text{Pt}(\text{dpb})\text{Cl}]$ (black), $[\text{Pt}(\text{Me}_2\text{dpb})\text{Cl}]$ (red), and $[\text{Pd}(\text{Me}_2\text{dpb})\text{Cl}]$ (blue) in 2-MeTHF at 298 K (left) and at 77 K as a glassy matrix (right). The Pd complex was not emissive at 298 K.

Table 3. Photoluminescence data of the investigated Pt and Pd complexes ^a.

	$[\text{Pt}(\text{dpb})\text{Cl}]$			$[\text{Pt}(\text{Me}_2\text{dpb})\text{Cl}]$			$[\text{Pd}(\text{Me}_2\text{dpb})\text{Cl}]$
	Solvent	DCM	2-MeTHF	DCM	2-MeTHF	2-MeTHF	
Temperature		298 K	298 K	298 K	298 K	77 K	77 K
$\lambda_{\text{Em}}/\text{nm}$		<u>490</u> , 523, 560sh	<u>494</u> , 526, 565sh	<u>495</u> , 527, 565	<u>498</u> , 530, 567sh	<u>489</u> , 503, 522, 560sh	<u>468</u> , 481, 501, 531sh
$\lambda_{\text{Exc}}/\text{nm}$		<u>289</u> , 330sh, 381, 403sh	<u>298</u> , 330sh, 388, 415	<u>295</u> , 335, 380, 410	<u>300</u> , 342, 390	<u>303</u> , 343, 373, 390	<u>300</u> , 347, 373
$\tau_{\text{av}}/\mu\text{s}$ ^b	Air-equilibrated	0.4464 ± 0.0015	0.1659 ± 0.0006	5.717 ± 0.016	0.3428 ± 0.0015	0.1185 ± 0.0006	152.8 ± 0.6
	Deaerated	6.050 ± 0.019	3.842 ± 0.009		6.420 ± 0.016	4.608 ± 0.010	5.794 ± 0.017 ^c [157 ± 3 (92); 102 ± 12 (8)] ^d
$\Phi_{\text{L}} \pm 0.02$	Air-equilibrated	0.04	<0.02	0.98	0.04	< 0.02	0.98
	Deaerated	0.64	0.52		0.75	0.64	

^a The Ni complex did not show any photoluminescence under these conditions. The Pd complex was not emissive at 298 K. ^b Photoluminescence decay measured at 495 nm, except: ^c 485 nm or ^d 470 nm (for multiexponential decays, the amplitude-weighted average lifetimes are given, as well as the different yields components in square brackets with their relative amplitudes indicated as percentages in parentheses). Photoluminescence quantum yields Φ_{L} . Main band maxima are underlined. Abbreviation: sh, shoulder.

The recorded data for the complexes $[\text{Pt}(\text{Me}_2\text{dpb})\text{Cl}]$ [60] and $[\text{Pt}(\text{dpb})\text{Cl}]$ [50,54,58,63,72] agreed very well with previous reports. Our results also confirm that the 3,5-dimethyl substitution does not markedly vary the photophysical properties of the parent $[\text{Pt}(\text{dpb})\text{Cl}]$ complex both at 298 K and at 77 K [60]. At 298 K, only a slight red-shift of about 250 cm^{-1} is found for the 3,5-Me₂ derivative, which vanishes at 77 K (Table 3). For the 4-Me derivative, a moderate red-shift of 565 cm^{-1} of the emission bands was previously reported at 298 K [50]. Moderate to marked blue-shifts had been found for the complexes involving the 4-MeOOC (423 cm^{-1}) [50], 3-F (424 cm^{-1}), and 3,5-F₂ (947 cm^{-1}) [54,58] substitution arrangements.

As observed for the absorption energies, the 3,4,5-F₃ or 3,5-(CF₃)₂ substitution pattern led to emission energies close to those of the parent complex [54]. Regardless of these shifts, neither the photoluminescence quantum yields (Φ_L) nor the excited states' lifetimes were markedly affected, the latter lying around 6 μ s in DCM (dichloromethane) and between 3.5 and 5 μ s in 2-MeTHF (2-methyl-tetrahydrofuran). At 77 K in frozen glassy matrices (2-MeTHF), both Pt complexes show a Φ_L of almost unity.

The Pd complex [Pd(Me₂dpb)Cl] did not show any PL at 298 K, but at 77 K we recorded structured excitation and emission spectra (Figure 6), which at first glance resembled to the corresponding Pt derivative. A closer inspection showed that the first emission maximum of the Pd complex is shifted to 468 nm if compared with the Pt complex (489 nm). In addition, the low-energy excitation maximum observed for Pd at 373 nm is blue-shifted if compared with the Pt complex (394 nm). The long lifetime of about 153 μ s recorded for the Pd complex can be explained by the smaller SOC, which dampens all the intrinsically spin-forbidden deactivation rates from the lowest triplet state. In fact, we found two components for the decay into the ground state with 157 μ s corresponding to the main component (92%) and about 102 μ s for a minor component (8%). Both of them are markedly longer-lived if compared with the analogous Pt complexes lying between 5 and 10 μ s, depending on the substitution pattern of the dpb ligand.

The most remarkable finding is the photoluminescence quantum yield of almost unity for the Pd complex. For the Pt derivative and the unsubstituted complex [Pt(dpb)Cl], the same values were found, which is in agreement with previous reports [50,54,58,60,63,72]. The Pd complex thus joins the small list of highly efficient Pd(II) complexes and very probably leads the short list of isoleptic Pt(II) and Pd(II) complexes for which Pd performs as good as Pt [13,24,27,28], while contrasting with the long list of Pt(II) outperforming their Pd(II) homologues [23,25,26,29–32,36,42,44]. The main reason for the outstanding performance of the Pd complex probably lies in the rigidity of the coordination environment and the significant ligand field splitting, which prevents radiationless deactivation processes. This calls for further dynamic quantum-chemical calculations, which will be part of future work on these complexes and derivatives with alternative co-ligands.

3. Materials and Methods

Instrumentation: ¹H, ¹³C, and correlation spectra were recorded on a Bruker Avance II 300 MHz (¹H: 300 MHz, ¹³C: 75 MHz), equipped with a double resonance (BBFO) 5 mm observe probe head with a z-gradient coil (Bruker, Rheinhausen, Germany). Chemical shifts were relative to TMS (¹H, ¹³C). UV-vis absorption spectra were recorded on a Varian Cary 05E spectrophotometer (Varian Medical Systems, Darmstadt, Germany). Elemental analyses were conducted using a HEKAtech CHNS EuroEA 3000 analyzer (HEKAtech, Wegberg, Germany). EI-MS spectra in the positive mode were measured using a Finnigan MAT 95 mass spectrometer. Simulations were performed using ISOPRO 3.0. Electrochemical measurements were carried out in 0.1 M *n*-Bu₄NPF₆ solution in THF (tetrahydrofuran) using a three-electrode configuration (glassy carbon electrode, Pt counter electrode, Ag/AgCl reference) and a Metrohm Autolab PGSTAT30 or μ Stat400 potentiostat (Metrohm, Filderstadt, Germany). The potentials were referenced against the ferrocene/ferrocenium redox couple as an internal standard. UV-vis-spectroelectrochemical measurements (in 0.1 M *n*-Bu₄NPF₆/THF solution) were performed using an optically transparent thin-layer electrode (OTTLE) cell [73] at room temperature.

Photophysical measurements: For the steady-state and time-resolved measurements, a FluoTime 300 spectrometer from PicoQuant was used. For the photoluminescence quantum yields, a Hamamatsu Photonics absolute PL quantum yield measurement system was used (Hamamatsu Photonics Deutschland GmbH, Geldern, Germany). All cuvettes used were round quartz cuvettes and the solvent 2-methyltetrahydrofuran (2-MeTHF) was purchased from abcr (Karlsruhe, Germany) in at least 99% purity and stabilised with 150–400 ppm BHT. The used dichloromethane (DCM) was of spectroscopic grade (Uvasol®).

Time-resolved luminescence decay curves are shown in Figures S15–S25. Further instrumental details can be found in the Supplementary Materials.

Single crystal structure analysis by X-ray diffractometry (XRD): The measurements were performed at 170(2) K, employing a Bruker D8 Venture including a Bruker Photon 100 CMOS detector using Mo-K α radiation ($\lambda = 0.71073 \text{ \AA}$) (Bruker, Rheinhausen, Germany). The crystal data was collected using APEX3 v2015.5-2 [74]. The structures were solved by dual space methods using SHELXT (Sheldrick 2015) [75] and the refinement was carried out with SHELXL 2017, employing the full-matrix least-squares methods on $F_0^2 \geq 2\sigma(F_0^2)$ [76]. The non-hydrogen atoms were refined with anisotropic displacement parameters without any constraints. The hydrogen atoms were included by using appropriate riding models. Data of the structure solutions and refinements can be obtained for [Ni(Me₂dpb)Cl]·CH₂Cl₂ (CCDC 2093819) and [Pd(Me₂dpb)Cl]·CH₂Cl₂ (CCDC 2095954) free of charge at <https://summary.ccdc.cam.ac.uk/structure-summary-form> (accessed on 19 August 2021) or from the Cambridge Crystallographic Data Centre, 12 Union Road, Cambridge, CB2 1EZ UK (Fax: +44-1223-336-033 or e-mail: deposit@ccdc.cam.ac.uk).

Quantum chemical calculations using density functional theory (DFT): All calculations were performed using the ORCA 4.2.1 program package [77,78]. Chemcraft 1.8 was used for the visualisation of results [79]. The geometries of the three complexes [M(Me₂dpb)Cl] (M = Ni, Pd, and Pt) were optimised using the BP86 functional, def2-TZVP basis sets, Grimme's D3 dispersion correction and the conductor-like screening model (COSMO) parametrised for THF [80–85]. For Pd and Pt, the def2-ECPs (ecp-28 and ecp-46, respectively) were used for the core electrons [86]. Subsequent frequency calculations on all three complexes yielded no imaginary modes, thus confirming the energetically minimal nature of the optimised geometries. Based on the optimised geometries, single point and TD-DFT [87] calculations using the Tamm–Dancoff approximation [88] were performed using the TPSSH hybrid functional [68,89]; def2-TZVP basis sets with def2-ECPs for Pd and Pt; Grimme's D3 dispersion correction; and the conductor-like screening model (COSMO) parametrised for THF. For each compound, 80 transitions were calculated. Molecular orbital energies and isosurfaces were extracted from the single point calculations.

Materials: 1,3-Di(pyridyl)benzene (dpbH) [47] and the complex [Pt(dpbc)Cl] [49] were synthesised as previously reported.

Synthesis of the protoligand 1,5-di(2-pyridyl)-2,4-dimethylbenzene (Me₂dpbH): Under inert conditions, a Schlenk flask was filled with 37.8 mL (60.5 mmol, 3.2 eq.) of a 1.6 M solution of *n*-butyl lithium diluted with 140 mL THF and cooled to $-78 \text{ }^\circ\text{C}$. A solution of 5.5 mL (56.7 mmol, 3.0 eq.) 2-bromopyridine in 20 mL THF was slowly added dropwise and stirred for 1 h. Afterwards, a suspension of 10.30 g (75.6 mmol, 4.0 eq.) ZnCl₂ (dried overnight at $140 \text{ }^\circ\text{C}$ under vacuum) in 60 mL THF was added to the reaction mixture and the reaction was warmed up to ambient temperature. Then, 1.09 g (0.95 mmol, 5 mol%) of [Pd(PPh₃)₄] and a solution of 5.00 g (18.9 mmol, 1.0 eq.) 1,5-dibromo-2,4-dimethylbenzene in 10 mL THF were added to the solution, which was then heated under reflux for 17 h. The reaction was terminated through the addition of 3.03 g (56.7 mmol, 2.9 eq.) NH₄Cl in 10 mL H₂O. The solution was extracted with EtOAc, the extract was washed with H₂O/brine, and the combined organic layers were dried over MgSO₄. After filtration, the solvents were evaporated and the product was purified by column chromatography with a *c*-Hex:EtOAc mixture (5:1 *v/v*). The product was obtained as a colourless solid (4.14 g, 15.88 mmol, 84%). $R_f = 0.137$ (*c*-Hex:EtOAc = 5:1). Elemental analysis found (calculated for C₁₈H₁₆N₂, $M = 260.34 \text{ g mol}^{-1}$): C, 83.07 (83.04); H, 6.13 (6.19); N, 10.66 (10.76). ¹H NMR (300 MHz, DMSO-*d*₆): $\delta = 8.67$ (ddd, 2H, $J = 4.8, 1.9, 1.0 \text{ Hz}$, H8,8'), 7.87 (td, 2H, $J = 7.7, 1.9 \text{ Hz}$, H6,6'), 7.57 (dt, 2H, $J = 7.9, 1.1 \text{ Hz}$, H5,5'), 7.46 (s, 1H, H9), 7.36 (ddd, 2H $J = 7.6, 4.8, 1.1 \text{ Hz}$, H7,7'), 7.26 (s, 1H, H1), 2.38 (s, 6H, CH₃) ppm. ¹³C NMR (75 MHz, DMSO-*d*₆): $\delta = 158.67$ (C4,4'), 149.00 (C8,8'), 137.68 (C3,3'), 136.51 (C6,6'), 135.23 (C2,2'), 133.13 (C1), 130.99 (C9), 123.92 (C5,5'), 121.88 (C7,7'), 19.82 (CH₃). EI-MS(+) $m/z = 259$ (100%) [M]⁺, 245 (95%) [M-CH₃]⁺, 182 (10%) [M-Py]⁺, 167 (10%) [M-Py-CH₃]⁺, 129 (20%) [M-L + Cl]⁺, 102 (5%) [M-Py-Py]⁺, 78 (5%) [Py]⁺.

Synthesis of [Ni(Me₂dpb)Cl]: In an inert flask equipped with a water trap filled with molecular sieve (3 Å), anhydrous 0.168 g NiCl₂ (1.3 mmol, 1.3 eq.), 0.100 g KOAc (1.0 mmol, 1.0 eq.), and 0.140 g K₂CO₃ (1.0 mmol, 1.0 eq.) were dried for 1 h in vacuum at 170 °C. Then, 0.26 g 1,5-di(2-pyridyl)-2,4-dimethylbenzene (1.0 mmol, 1.0 eq.) and dry *p*-xylene (200 mL) were added and heated under reflux for 72 h. After cooling to ambient temperature, the precipitated solid was filtered off, washed once with *p*-xylene, and the product was extracted using THF and washed with CH₂Cl₂ afterwards. The solvent was removed and the dark orange product was isolated. Careful crystallisation of the *p*-xylene fraction gave further product. Total yield: 0.319 g (0.94 mmol, 94%). Elemental analysis found (calculated for C₁₈H₁₅N₂NiCl, M = 353.48 g mol⁻¹): C, 61.20 (61.16); H, 4.36 (4.28); N, 7.96 (7.93). ¹H NMR (300 MHz, CD₂Cl₂): δ = 8.84 (br s, 2H, H8,8'), 7.81 (td, 2H, J = 7.8, 1.7 Hz, H6,6'), 7.65 (d, 2H, J = 8.1 Hz, H5,5'), 7.09 (ddd, 2H, J = 7.3, 5.8, 1.4 Hz, H7,7'), 6.71 (s, 1H, H1), 2.55 (s, 6H, CH₃) ppm. ¹³C NMR (75 MHz, CD₂Cl₂): δ = 167.02 (not assigned), 164.55 (not assigned), 139.24 (C6,6'), 135.33 (not assigned), 132.65 (C1), 122.07 (C7,7'), 121.55 (C5,5'), 21.79 (CH₃) ppm. EI-MS(+) *m/z* = 352 (25%) [M]⁺, 317 (100%) [M-Cl]⁺, 259 (25%) [M-NiCl]⁺, 245 (25%) [M-NiCl-CH₃]⁺, 229 (5%) [PyPhPy]⁺, 180 (5%) [M-NiCl-Py]⁺, 167 (5%) [PyPhCH₃]⁺, 151 (5%) [PhPy]⁺, 129 (5%) [M-L + Cl]⁺.

Synthesis of [Pd(Me₂dpb)Cl]: In an inert flask equipped with a water trap filled with molecular sieves (3 Å), 0.186 g [Pd(COD)Cl₂] (0.65 mmol, 1.3 eq.), 0.491 g KOAc (0.5 mmol, 1.0 eq.), and 0.693 g K₂CO₃ (0.5 mmol, 1.0 eq.) were prepared and 0.130 g 1,5-di(2-pyridyl)-2,4-dimethylbenzene (0.5 mmol, 1.0 eq.) as well as dry *p*-xylene (120 mL) were added and heated under reflux for 72 h under the strict exclusion of light. After cooling to ambient temperature, the precipitated greyish-yellow solid was filtered off, washed once with *p*-xylene, and the product was extracted using CH₂Cl₂. The solvent was removed and the pale orange solid was isolated (0.178 g, 0.44 mmol, 68%). Elemental analysis found (calculated for C₁₈H₁₅N₂PdCl, M = 401.20 g mol⁻¹): C, 53.82 (53.89); H, 4.27 (4.28); and N, 6.94 (6.98). ¹H NMR (300 MHz, CD₂Cl₂): δ = 9.09 (d, 2H, J = 4.8 Hz, H8,8'), 7.85 (td, 2H, J = 7.8, 7.3, 1.7 Hz, H6,6'), 7.79 (d, 2H, J = 7.8 Hz, H5,5'), 7.18 (ddd, 2H, J = 7.1, 5.4, 1.4 Hz, H7,7'), 6.65 (s, 1H, H1), and 2.55 (s, 6H, CH₃) ppm. ¹³C NMR (75 MHz, CD₂Cl₂): δ = 177.17 (not assigned), 173.98 (not assigned), 152.88 (C8,8'), 139.23 (C6,6'), 136.77 (not assigned), 132.62 (C1), 122.79 (C7,7'), 122.67 (C5,5'), and 22.67 (CH₃) ppm. EI-MS(+) *m/z* = 400 (20%) [M]⁺, 365 (100%) [M-Cl]⁺, 259 (100%) [M-PdCl]⁺, 245 (40%) [M-PdCl-CH₃]⁺, 229 (5%) [PyPhPy]⁺, 180 (10%) [M-PdCl-Py]⁺, 167 (10%) [PyPhCH₃]⁺, 151 (5%) [PhPy]⁺, and 78 (5%) [Py]⁺.

Synthesis of [Pt(Me₂dpb)Cl]: 0.166 g (0.40 mmol, 1.0 eq.) K₂PtCl₄ and 0.104 g (0.4 mmol, 1.0 eq.) 1,5-di(2-pyridyl)-2,4-dimethylbenzene were suspended in 15 mL glacial acetic acid and refluxed for 3 d. The reaction mixture was then cooled down to room temperature and the precipitated bright orange solid was filtered off, washed with MeOH, H₂O, EtOH and Et₂O, and dried over P₄O₁₀ at a reduced pressure yielding 0.135 mg (0.28 mmol, 70%). Elemental analysis found (calculated for C₁₈H₁₅N₂PtCl, M = 489.87 g mol⁻¹): C, 43.14 (44.13); H, 3.06 (3.09); N, 5.75 (5.72). ¹H NMR (300 MHz, CD₂Cl₂): δ = 9.39 (dd, 2H, J = 5.7, 2.3 Hz, J_{PH} = 42 Hz, H8,8'), 7.93 (ddd, 2H, J = 7.8, 7.3, 1.8 Hz, H6,6'), 7.85 (d, 2H, J = 7.7 Hz, H5,5'), 7.24 (ddd, 2H, J = 7.4, 5.7, 1.6 Hz, H7,7'), 6.79 (s, 1H, H1), 2.64 (s, 6H, CH₃) ppm. ¹³C NMR (75 MHz, CD₂Cl₂): δ = 168.83, 164.19 (not assigned), 152.49 (C8,8'), 139.37 (C6,6'), 137.27 (not assigned), 131.19 (C1), 123.00 (C7,7'), 122.83 (C5,5'), 22.27 (CH₃) ppm. ¹⁹⁵Pt NMR (64 MHz, DMSO-*d*₆): δ = -3609.20. EI-MS(+) *m/z* = 489 (60%) [M]⁺, 454 (100%) [M-Cl]⁺, 438 (20%) [M-Cl-CH₃]⁺, 424 (10%) [M-Cl-2CH₃]⁺, 259 (60%) [M-PtCl]⁺, 245 (60%) [M-PtCl-CH₃]⁺, 229 (5%) [PyPhPy]⁺, 180 (10%) [M-PtCl-Py]⁺, 167 (10%) [PyPhCH₃]⁺, 151 (5%) [PhPy]⁺, 78 (5%) [Py]⁺.

Alternative synthesis of [Pd(Me₂dpb)Cl]: 0.112 g (0.43 mmol, 1.0 eq.) of 1,5-di(2-pyridyl)-2,4-dimethylbenzene and 0.140 g (0.43 mmol, 1.0 eq.) K₂[PdCl₄] were suspended in 30 mL HOAc and heated under reflux for 22 h. The precipitated solid was filtered; washed with HOAc, MeOH, and Et₂O (20 mL each), and then dried under vacuum. The product was isolated as a pale orange solid (0.168 g, 0.42 mmol, 98%). Elemental analysis

found (calculated for $C_{18}H_{15}N_2PdCl$, $M = 401.20 \text{ g mol}^{-1}$): C, 53.88 (53.89); H, 4.29 (4.28); N, 6.97 (6.98). NMR and MS characterisation gave identical values to those reported above.

Attempted syntheses of [Pd(dpb)Cl]: We also tried to cyclopalladate the unsubstituted 1,3-dipyridyl-benzene (dpbH) protoligand using our base-assisted method, starting from the Pd precursors $PdCl_2$, $K_2[PdCl_4]$, or $[Pd(COD)Cl_2]$ (Scheme S1). However, the target complex was not obtained. Instead, we isolated the previously reported tetranuclear complex $[Pd_4(\mu-\kappa^2, \kappa^2 dpb)_2(\mu-\kappa^1, \kappa^1-OAc)_4]$ (see Scheme 2) and its unprecedented pivalate derivative. Details are provided in the Supplementary Materials.

4. Conclusions

In this study, we completed the series of homologous complexes $[M(Me_2dpb)Cl]$ containing the tridentate *N,C,N*-coordinating 3,5-dimethyl-2,6-dipyridyl-phenide ligand (Me_2dpb^-) by adding the Ni(II) and Pd(II) derivatives to the previously reported Pt(II) complex. All three complexes were synthesised using a base-assisted C-H activation method starting from the protoligand 1,5-di(2-pyridyl)-2,4-dimethylbenzene (Me_2dpbH), metal chlorides, and KOAc and K_2CO_3 in vigorously dried *p*-xylene.

Quite invariant electrochemical reductions around -2.3 V are essentially constant and DFT calculations confirmed the expected ligand- π^* -centred reductions. The lowest unoccupied molecular orbital (LUMO) for all three complexes is very similar and the DFT-calculated energies of about -2.3 eV perfectly match the experimental results when using the TPSSh functional. The oxidation potentials increased along the series $Pt < Ni < Pd$ from 0.15 to 0.74 V and the DFT-calculated highest occupied molecular orbitals (HOMO) confirm the marked contributions from metal d_{yz} orbitals alongside with phenyl C4, C2, C1, and C6, and Cl p_z contributions. As expected, the d_z^2 (HOMO-1 for Ni) is stabilised for the Pd and Pt derivative while the anti-bonding $d_x^2 - y^2$ orbital is destabilised in line with the larger ligand field splitting of Pd and Pt.

The experimental long-wavelength UV-vis absorption energies increased along the series $Ni < Pt < Pd$, matching well with the observed colours of the compounds ranging from red to yellow. The TD-DFT calculated absorption energies are only slightly red-shifted if compared with the experimental data. The lowest-energy transition calculated for the Ni complex has a pronounced d_z^2 -type contribution to the overall metal-to-ligand charge transfer (MLCT) character of the excited configuration. For the Pt and Pd compounds, the d_z^2 is energetically not available and strongly mixed Cl-to- π^* /phenyl-to- π^* /M(d_{yz})-to- π^* (XLCT/ILCT/MLCT) states were found. Contributions of the antibonding metal $d_x^2 - y^2$ orbitals to dissociative states were found for Ni at around 390 nm (3.18 eV), while such states were found at 281 nm (4.41 eV) for Pd and at 255 nm (4.86 eV) for Pt, in line with the expected trends regarding the ligand field splitting. The observed lowest energy absorption bands were assigned to the almost purely (95%) HOMO \rightarrow LUMO+1 configurations for the Pt and Pd complexes, based on the calculated vertical $S_0 \rightarrow S_1$ transitions; for the Ni derivative, the transition leads to an excited state with the HOMO-2 \rightarrow LUMO (52%) and HOMO \rightarrow LUMO+1 (43%) character that matches well with the observed long-wavelength bands. The HOMO \rightarrow LUMO (for Pt and Pd) and HOMO-1 \rightarrow LUMO (Ni) states were assigned to absorptive transitions with low probability and match very well the so-called optical cut-off in the spectra. This confirms the versatility of the TPSSh functional for the full Ni-Pd-Pt triad.

The previously reported Pt complex $[Pt(Me_2dpb)Cl]$ showed triplet luminescence at 498 nm in fluid 2-Me-THF solutions at 298 K, which shifted to 489 nm in frozen glassy 2-MeTHF matrices at 77 K. The Pd derivative showed a structured emission profile at 77 K, peaking at 468 nm with an outstanding PL quantum yield reaching unity, as observed for the Pt derivative and the unsubstituted Pt complex $[Pt(dpb)Cl]$. No emission was observed for the Ni complex at 77 or at 298 K in any form (solution or solids). This is in agreement with the above-mentioned dissociative states at relatively low energies below 3.18 eV with contributions of a metal-centred character to the excited configurations, promoting rapid radiationless relaxation to the ground state. For the Pd(II) and Pt(II)

derivatives, such “dark states” lie at markedly higher energies, namely above 4.41 eV for Pd and above 4.86 eV for Pt. Remarkably, the calculated vertical $S_0 \rightarrow S_1$ transitions show excited states with a contribution of the configuration involving the LUMO+4 for Pd (71%) and a markedly lower participation of the LUMO+5 on the excited state for Pt (38%), which is in line with the very different behaviour at 298 K. The more efficient radiationless decay of the Pd complex at 298 K is attributed to this higher antibonding $d_{x^2-y^2}$ -orbital participation if compared with the analogous Pt derivative. In contrast to this, at 77 K, the quite similar energies of the “dark” states for Pt and Pd are decisive, leading to very similar photoluminescence patterns.

In any case, the similar PL efficiency for a Pd(II) complex with its Pt(II) homologue is remarkable and rarely encountered. We will thus use the observed balance of energy + character + dynamics of excited states to design more Pd(II) complexes with efficient PL in future work.

Supplementary Materials: The following information is available online: Supplementary Material contains 25 Figures and 21 Tables with crystal and molecular structures, cyclic voltammograms, UV-vis absorption spectra, steady-state photoluminescence spectra and time-resolved photoluminescence decays, as well as UV-vis absorption spectra of reduced and oxidised species; Supplementary Material II contains 27 Figures with NMR and MS characterisation of Ni, Pd, and Pt complexes including Pd side-products.

Author Contributions: Conceptualisation, A.K.; methodology, L.K., R.J., C.A.S. and A.K.; investigation, L.K., R.J., A.S.K. and S.B.; resources, A.K. and C.A.S.; data curation, L.K., R.J., A.S.K. and S.B.; visualisation, L.K., R.J., S.B. and A.K.; supervision and project administration, C.A.S. and A.K.; manuscript original draft, L.K., R.J. and A.K.; manuscript editing, A.K. and C.A.S. All authors have read and agreed to the published version of the manuscript.

Funding: This research was funded by the Deutsche Forschungsgemeinschaft (DFG Priority Programme 2102 “Light-controlled Reactivity of Metal Complexes”), STR 1186/6-1 (CAS) and KL1194/16-1 (AK).

Institutional Review Board Statement: Not applicable.

Informed Consent Statement: Not applicable.

Data Availability Statement: Data might be requested directly from the authors.

Acknowledgments: At the Department of Chemistry, University of Cologne, we thank Daniele Cuzzupe and André Zenz for helping with the syntheses; Silke Kremer (XRD facility) for measuring XRD datasets; and Sean S. Sebastian for the assistance in the refinement of the XRD data. The Regional Computing Centre of the University of Cologne (RRZK) is acknowledged for providing computing time on the DFT-funded High-Performance Computing (HPC) system CHEOPS, as well as for the support.

Conflicts of Interest: The authors declare no competing financial interest.

Sample Availability: Samples of the compounds are not available.

References

1. Mori, K.; Yamashita, H. Metal Complexes Supported on Solid Matrices for Visible-Light-Driven Molecular Transformations. *Chem. Eur. J.* **2016**, *22*, 11122–11137. [[CrossRef](#)]
2. Parasram, M.; Gevorgyan, V. Visible light-induced transition metal-catalyzed transformations: Beyond conventional photosensitizers. *Chem. Soc. Rev.* **2017**, *46*, 6227–6240. [[CrossRef](#)]
3. Guerchais, V.; Fillaut, J.-L. Sensory luminescent iridium(III) and platinum(II) complexes for cation recognition. *Coord. Chem. Rev.* **2011**, *255*, 2448–2457. [[CrossRef](#)]
4. Zhao, Q.; Li, F.; Huang, C. Phosphorescent chemosensors based on heavy-metal complexes. *Chem. Soc. Rev.* **2010**, *39*, 3007–3030. [[CrossRef](#)]
5. Kalinowski, J.; Fattori, V.; Cocchi, M.; Gareth Williams, J.A. Light-emitting devices based on organometallic platinum complexes as emitters. *Coord. Chem. Rev.* **2011**, *255*, 2401–2425. [[CrossRef](#)]
6. Li, K.; Tong, G.S.M.; Wan, Q.; Cheng, G.; Tong, W.-Y.; Ang, W.-H.; Kwong, W.-L.; Che, C.-M. Highly phosphorescent platinum(II) emitters: Photophysics, materials and biological application. *Chem. Sci.* **2016**, *7*, 1653–1673. [[CrossRef](#)]

7. Yam, V.W.-W.; Law, A.S.-Y. Luminescent d^8 metal complexes of platinum(II) and gold(III): From photophysics to photofunctional materials and probes. *Coord. Chem. Rev.* **2020**, *414*, 213298. [[CrossRef](#)]
8. Fantacci, S.; De Angelis, F. A computational approach to the electronic and optical properties of Ru(II) and Ir(III) polypyridyl complexes: Applications to DSC, OLED and NLO. *Coord. Chem. Rev.* **2011**, *255*, 2704–2726. [[CrossRef](#)]
9. Housecroft, C.E.; Constable, E.C. Over the LEC rainbow: Colour and stability tuning of cyclometallated iridium(III) complexes in light-emitting electrochemical cells. *Coord. Chem. Rev.* **2017**, *350*, 155–177. [[CrossRef](#)]
10. Zhang, Y.; Wang, Y.; Song, J.; Qu, J.; Li, B.; Zhu, W.; Wong, W.-Y. Near-Infrared Emitting Materials via Harvesting Triplet Excitons: Molecular Design, Properties, and Application in Organic Light Emitting Diodes. *Adv. Opt. Mater.* **2018**, *6*, 1800466. [[CrossRef](#)]
11. Yersin, H.; Rausch, A.F.; Czerwieniec, R.; Hofbeck, T.; Fischer, T. The triplet state of organo-transition metal compounds. Triplet harvesting and singlet harvesting for efficient OLEDs. *Coord. Chem. Rev.* **2011**, *255*, 2622–2652. [[CrossRef](#)]
12. Bizzarri, C.; Spuling, E.; Knoll, D.M.; Volz, D.; Bräse, S. Sustainable metal complexes for organic light-emitting diodes (OLEDs). *Coord. Chem. Rev.* **2018**, *373*, 49–82. [[CrossRef](#)]
13. Fleetham, T.; Li, G.; Li, J. Phosphorescent Pt(II) and Pd(II) Complexes for Efficient, High-Color-Quality, and Stable OLEDs. *Adv. Mater.* **2017**, *29*, 1601861. [[CrossRef](#)] [[PubMed](#)]
14. Archer, S.; Weinstein, J.A. Charge-separated excited states in platinum(II) chromophores: Photophysics, formation, stabilization and utilization in solar energy conversion. *Coord. Chem. Rev.* **2012**, *256*, 2530–2561. [[CrossRef](#)]
15. Strassner, T. Phosphorescent Platinum(II) Complexes with C^*C^* Cyclometalated NHC Ligands. *Acc. Chem. Res.* **2016**, *49*, 2680–2689. [[CrossRef](#)]
16. Cebrián, C.; Mauro, M. Recent advances in phosphorescent platinum complexes for organic light-emitting diodes. *Beilstein J. Org. Chem.* **2018**, *14*, 1459–1481. [[CrossRef](#)]
17. Koshevoy, I.O.; Krause, M.; Klein, A. Non-Covalent Intramolecular Interactions through Ligand-Design Promoting Efficient Luminescence from Transition Metal Complexes. *Coord. Chem. Rev.* **2020**, *405*, 213094. [[CrossRef](#)]
18. Sivchik, V.; Kochetov, A.; Eskelinen, T.; Kisel, K.S.; Solomatina, A.I.; Grachova, E.V.; Tunik, S.P.; Hirva, P.; Koshevoy, I.O. Modulation of Metallophilic and p–p Interactions in Platinum Cyclometalated Luminophores with Halogen Bonding. *Chem. Eur. J.* **2021**, *27*, 1787–1794. [[CrossRef](#)]
19. Ravotto, L.; Ceroni, P. Aggregation induced phosphorescence of metal complexes: From principles to applications. *Coord. Chem. Rev.* **2017**, *346*, 62–76. [[CrossRef](#)]
20. Gray, H.B.; Záliš, S.; Vlček, A. Electronic structures and photophysics of d^8 - d^8 complexes. *Coord. Chem. Rev.* **2017**, *345*, 297–317. [[CrossRef](#)]
21. Ganesan, P.; Hung, W.; Tso, J.; Ko, C.; Wang, T.; Chen, P.; Hsu, H.; Liu, S.; Lee, G.; Chou, P.; et al. Functional Pyrimidinyl Pyrazolate Pt(II) Complexes: Role of Nitrogen Atom in Tuning the Solid-State Stacking and Photophysics. *Adv. Funct. Mater.* **2019**, *29*, 1900923. [[CrossRef](#)]
22. Cinninger, L.M.; Bastatas, L.D.; Shen, Y.; Holliday, B.J.; Slinker, J.D. Luminescent properties of a 3,5-diphenylpyrazole-bridged Pt(II) dimer. *Dalton Trans.* **2019**, *48*, 9684–9691. [[CrossRef](#)]
23. Yam, V.W.-W.; Au, V.K.-M.; Leung, S.Y.-L. Light-Emitting Self-Assembled Materials Based on d^8 and d^{10} Transition Metal Complexes. *Chem. Rev.* **2015**, *115*, 7589–7728. [[CrossRef](#)]
24. Zou, C.; Lin, J.; Suo, S.; Xie, M.; Chang, X.; Lu, W. Palladium(II) *N*-heterocyclic allenylidene complexes with extended intercationic Pd···Pd interactions and MMLCT phosphorescence. *Chem. Commun.* **2018**, *54*, 5319–5322. [[CrossRef](#)] [[PubMed](#)]
25. Santana, M.D.; López-Banet, L.; Sánchez, G.; Pérez, J.; Pérez, E.; García, L.; Serrano, J.L.; Espinosa, A. Non-covalent stacking interactions directing the structural and photophysical features of mono- and dinuclear cyclometalated palladium(II) complexes. *Dalton Trans.* **2016**, *45*, 8601–8613. [[CrossRef](#)]
26. Liu, L.; Wang, X.; Hussain, F.; Zeng, C.; Wang, B.; Li, Z.; Kozin, I.; Wang, S. Multiresponsive Tetradentate Phosphorescent Metal Complexes as Highly Sensitive and Robust Luminescent Oxygen Sensors: Pd(II) Versus Pt(II) and 1,2,3-Triazolyl Versus 1,2,4-Triazolyl. *ACS Appl. Mater. Interfaces* **2019**, *11*, 12666–12674. [[CrossRef](#)]
27. Chow, P.-K.; Cheng, G.; Tong, G.S.-M.; Ma, C.; Kwok, W.-M.; Ang, W.-H.; Chung, C.Y.-S.; Yang, C.; Wang, F.; Che, C.-M. Highly luminescent palladium(II) complexes with sub-millisecond blue to green phosphorescent excited states. Photocatalysis and highly efficient PSF-OLEDs. *Chem. Sci.* **2016**, *7*, 6083–6098. [[CrossRef](#)]
28. Fleetham, T.; Ji, Y.; Huang, L.; Fleetham, T.S.; Li, J. Efficient and stable single-doped white OLEDs using a palladium-based phosphorescent excimer. *Chem. Sci.* **2017**, *8*, 7983–7990. [[CrossRef](#)]
29. Lin, J.; Zou, C.; Zhang, X.; Gao, Q.; Suo, S.; Zhuo, Q.; Chang, X.; Xie, M.; Lu, W. Highly phosphorescent organopalladium(II) complexes with metal–metal-to-ligand charge-transfer excited states in fluid solutions. *Dalton Trans.* **2019**, *48*, 10417–10421. [[CrossRef](#)]
30. Krause, M.; Von der Stück, R.; Brünkink, D.; Buss, S.; Doltsinis, N.L.; Strassert, C.A.; Klein, A. Platinum and palladium complexes of tridentate C^*N^*N (phen-ide)-pyridine-thiazol ligands—A case study involving spectroelectrochemistry, photoluminescence spectroscopy and TD-DFT calculations. *Inorg. Chim. Acta* **2021**, *518*, 120093. [[CrossRef](#)]
31. Föllner, J.; Friese, D.H.; Riese, S.; Kaminski, J.M.; Metz, S.; Schmidt, D.; Würthner, F.; Lambert, C.; Marian, C.M. On the photophysical properties of Ir^{III}, Pt^{II}, and Pd^{II} (phenylpyrazole) (phenyldipyrrin) complexes. *Phys. Chem. Chem. Phys.* **2020**, *22*, 3217–3233. [[CrossRef](#)]

32. Eskelinen, T.; Buss, S.; Petrovskii, S.K.; Grachova, E.V.; Krause, M.; Klein, A.; Strassert, C.A.; Koshevoy, I.O.; Hirva, P. Photophysics and Excited State Dynamics of Cyclometalated $[M(C^*N^*N)(CN)]$ ($M = Ni, Pd, Pt$) Complexes: A Theoretical and Experimental Study. *Inorg. Chem.* **2021**, *60*, 8777–8789. [[CrossRef](#)]
33. Wong, Y.-S.; Tang, M.-C.; Ng, M.; Yam, V.W.-W. Toward the Design of Phosphorescent Emitters of Cyclometalated Earth-Abundant Nickel(II) and Their Supramolecular Study. *J. Am. Chem. Soc.* **2020**, *142*, 7638–7646. [[CrossRef](#)] [[PubMed](#)]
34. Chou, P.T.; Chi, Y.; Chung, M.-W.; Lin, C.-C. Harvesting luminescence via harnessing the photophysical properties of transition metal complexes. *Coord. Chem. Rev.* **2011**, *255*, 2653–2665. [[CrossRef](#)]
35. Tong, G.S.-M.; Che, C.-M. Emissive or Nonemissive? A Theoretical Analysis of the Phosphorescence Efficiencies of Cyclometalated Platinum(II) Complexes. *Chem. Eur. J.* **2009**, *15*, 7225–7237. [[CrossRef](#)]
36. Liu, Y.-T.; Li, Y.-R.; Wang, X.; Bai, F.-Q. Theoretical investigation of N^*C^*N -coordinated Pt(II) and Pd(II) complexes for long-lived two-photon photodynamic therapy. *Dyes Pigm.* **2017**, *142*, 55–61. [[CrossRef](#)]
37. Haque, A.; Xu, L.; Al-Balushi, R.A.; Al-Suti, M.K.; Ilmi, R.; Guo, Z.; Khan, M.S.; Wong, W.-Y.; Raithby, P.R. Cyclometallated tridentate platinum(II) arylacetylide complexes: Old wine in new bottles. *Chem. Soc. Rev.* **2019**, *48*, 5547–5563. [[CrossRef](#)] [[PubMed](#)]
38. Gareth Williams, J.A. The coordination chemistry of dipyritylbenzene: N-deficient terpyridine or panacea for brightly luminescent metal complexes? *Chem. Soc. Rev.* **2009**, *38*, 1783–1801. [[CrossRef](#)]
39. Garbe, S.; Krause, M.; Klimpel, A.; Neundorf, I.; Lippmann, P.; Ott, I.; Brünkink, D.; Strassert, C.A.; Doltsinis, N.L.; Klein, A. Cyclometalated Pt Complexes of CNC Pincer Ligands: Luminescence and Cytotoxic Evaluation. *Organometallics* **2020**, *39*, 746–756. [[CrossRef](#)]
40. Hebenbrock, M.; Stegemann, L.; Kösters, N.L.; Doltsinis, N.L.; Müller, J.; Strassert, C.A. Phosphorescent Pt(II) complexes bearing a monoanionic C^*N^*N luminophore and tunable ancillary ligands. *Dalton Trans.* **2017**, *46*, 3160–3169. [[CrossRef](#)]
41. Cnudde, M.; Brünkink, D.; Doltsinis, N.L.; Strassert, C.A. Tetradentate $N^*N^*N^*N^*$ -type luminophores for Pt(II) complexes: Synthesis, photophysical and quantum-chemical investigation. *Inorg. Chim. Acta* **2021**, *518*, 120090. [[CrossRef](#)]
42. Lai, S.-W.; Cheung, T.-C.; Chan, M.C.W.; Cheung, K.-K.; Peng, S.-M.; Che, C.-M. Luminescent Mononuclear and Binuclear Cyclometalated Palladium(II) Complexes of 6-Phenyl-2,2'-bipyridines: Spectroscopic and Structural Comparisons with Platinum(II) Analogues. *Inorg. Chem.* **2000**, *39*, 255–262. [[CrossRef](#)]
43. Cheung, T.-C.; Cheung, K.-K.; Peng, S.-M.; Che, C.-M. Photoluminescent cyclometallated diplatinum(II,II) complexes: Photophysical properties and crystal structures of $[PtL(PPh_3)]ClO_4$, and $[Pt_2L_2(\mu-dppm)]ClO_4$ ($HL = 6$ -phenyl-2,2'-bipyridine, $dppm = Ph_2PCH_2PPh_2$). *J. Chem. Soc. Dalton Trans.* **1996**, *8*, 1645–1651. [[CrossRef](#)]
44. Karlen, T.; Ludi, A.; Güdel, H.U. One-Dimensional Migration of 3MLCT Excitation Energy in $Pd^{II}(phbpy)Cl$ ($phbpy = 6$ -Phenyl-2,2'-bipyridine). *Inorg. Chem.* **1991**, *10*, 2249–2250. [[CrossRef](#)]
45. Niazi, M.; Klein, A. DFT Investigation of the Molecular Properties of the Dimethylglyoximate Complexes $[M(Hdmg)_2]$ ($M = Ni, Pd, Pt$). *Inorganics* **2021**, *9*, 47. [[CrossRef](#)]
46. Haseloer, A.; Jordan, R.; Denkler, L.M.; Reimer, M.; Olthof, S.; Schmidt, I.; Meerholz, K.; Hörner, G.; Klein, A. Ni, Pd, and Pt complexes of a tetradentate dianionic thiosemicarbazone-based $O^*N^*N^*S$ ligand. *Dalton Trans.* **2021**, *50*, 4311–4322. [[CrossRef](#)] [[PubMed](#)]
47. Kletsch, L.; Hörner, G.; Klein, A. Cyclometalated Ni(II) complexes $[Ni(N^*C^*N)X]$ of the tridentate 2,6-di(2-pyridyl)-phen-ide ligand. *Organometallics* **2020**, *39*, 2820–2829. [[CrossRef](#)]
48. Vogt, N.; Sivchik, V.; Sandleben, A.; Hörner, G.; Klein, A. Direct Base-Assisted C-H Cyclonickelation of 6-Phenyl-2,2'-bipyridine. *Molecules* **2020**, *25*, 997. [[CrossRef](#)]
49. Cardenas, D.J.; Echavarren, A.M.; Ramirez de Arellano, M.C. Divergent Behavior of Palladium(II) and Platinum(II) in the Metalation of 1,3-Di(2-pyridyl)benzene. *Organometallics* **1999**, *18*, 3337–3341. [[CrossRef](#)]
50. Gareth Williams, J.A.; Beeby, A.; Davies, E.S.; Weinstein, J.A.; Wilson, C. An Alternative Route to Highly Luminescent Platinum(II) Complexes: Cyclometalation with N^*C^*N -Coordinating Dipyritylbenzene Ligands. *Inorg. Chem.* **2003**, *42*, 8609–8611. [[CrossRef](#)]
51. Hofmann, A.; Dahlenburg, L.; Van Eldik, R. Cyclometalated Analogues of Platinum Terpyridine Complexes: Kinetic Study of the Strong σ -Donor Cis and Trans Effects of Carbon in the Presence of a π -Acceptor Ligand Backbone. *Inorg. Chem.* **2003**, *42*, 6528–6538. [[CrossRef](#)]
52. Soro, B.; Stoccoro, S.; Minghetti, G.; Zucca, A.; Cinellu, M.A.; Manassero, M.; Gladiali, S. The first pincer-aryl $[M-(NCN)]$ complexes ($M = Pd(II); Pt(II)$) with chiral pyridine donors: Synthesis and catalytic activity in C–C bond formation. *Inorg. Chim. Acta* **2006**, *359*, 1879–1888. [[CrossRef](#)]
53. Abe, T.; Shinozaki, K.; Ikeda, N.; Suzuki, T. [2,6-Bis(5-methyl-2-pyridyl)phenyl- κ^3N, C^1, N']chloridoplatinum(II). *Acta Cryst. C Cryst. Struct. Commun.* **2007**, *C63*, m456–m458. [[CrossRef](#)]
54. Wang, Z.; Turner, E.; Mahoney, V.; Madakuni, S.; Groy, T.; Li, J. Facile Synthesis and Characterization of Phosphorescent $Pt(N^*C^*N)X$ Complexes. *Inorg. Chem.* **2010**, *49*, 11276–11286. [[CrossRef](#)]
55. Soro, B.; Stoccoro, S.; Minghetti, G.; Zucca, A.; Cinellu, M.A.; Gladiali, S.; Manassero, M.; Sansoni, M. Synthesis of the First C-2 Cyclopalladated Derivatives of 1,3-Bis(2-pyridyl)benzene. Crystal Structures of $[Hg(N-C-N)Cl]$, $[Pd(N-C-N)Cl]$, and $[Pd_2(N-C-N)_2(\mu-OAc)_2][Hg_2Cl_6]$. Catalytic Activity in the Heck Reaction. *Organometallics* **2005**, *24*, 53–61. [[CrossRef](#)]

56. Constable, E.C.; Henney, R.P.G.; Leese, T.A. Cyclometallation Reactions of 6-Phenyl-2,2'-bipyridine; a Potential C,N,N-Donor Analogue of 2,2':6', 2''-Terpyridine. Crystal and Molecular Structure of Dichlorobis(6-phenyl-2,2'-bipyridine)ruthenium(II). *J. Chem. Soc. Dalton Trans.* **1990**, 443–449. [CrossRef]
57. Yamamoto, K.; Higuchi, K.; Ogawa, M.; Sogawa, H.; Kuwata, S.; Hayashi, Y.; Kawauchi, S.; Takata, T. Macrocyclic Metal Complexes Bearing Rigid Polyaromatic Ligands: Synthesis and Catalytic Activity. *Chem. Asian J.* **2020**, *15*, 356–359. [CrossRef]
58. Iwakiri, A.; Konno, Y.; Shinozaki, K. Determination of excimer emission quantum yield of Pt(dpb)Cl (dpbH = 1,3-di(2-pyridyl)benzene and its analogues in solution. *J. Lumin.* **2019**, *207*, 482–490. [CrossRef]
59. Garoni, E.; Boixel, J.; Dorcet, V.; Roisnel, T.; Roberto, D.; Jacquemin, D.; Guerchais, V. Controlling the emission in flexibly-linked (N⁺C⁻N)platinum dyads. *Dalton Trans.* **2018**, *47*, 224–232. [CrossRef]
60. Schulze, B.; Friebe, C.; Jäger, M.; Görls, H.; Birkner, E.; Winter, A.; Schubert, U.S. Pt^{II} Phosphors with Click-Derived 1,2,3-Triazole-Containing Tridentate Chelates. *Organometallics* **2018**, *37*, 145–155. [CrossRef]
61. Rodrigue-Witchel, A.; Rochester, D.L.; Zhao, S.-B.; Lavelle, K.B.; Gareth Williams, J.A.; Wang, S.; Connick, W.B.; Reber, C. Pressure-induced variations of MLCT and ligand-centered luminescence spectra in square-planar platinum(II) complexes. *Polyhedron* **2016**, *108*, 151–155. [CrossRef]
62. Rausch, A.F.; Murphy, L.; Gareth Williams, J.A.; Yersin, H. Improving the Performance of Pt(II) Complexes for Blue Light Emission by Enhancing the Molecular Rigidity. *Inorg. Chem.* **2012**, *51*, 312–319. [CrossRef]
63. Rausch, A.F.; Murphy, L.; Gareth Williams, J.A.; Yersin, H. Probing the Excited State Properties of the Highly Phosphorescent Pt(dpyb)Cl Compound by High-Resolution Optical Spectroscopy. *Inorg. Chem.* **2009**, *48*, 11407–11414. [CrossRef]
64. Abe, T.; Itakura, T.; Ikeda, N.; Shinozaki, K. Luminescence color change of a platinum(II) complex solid upon mechanical grinding. *Dalton Trans.* **2009**, *1*, 711–715. [CrossRef]
65. Farley, S.J.; Rochester, D.L.; Thompson, A.L.; Howard, J.A.K.; Gareth Williams, J.A. Controlling Emission Energy, Self-Quenching, and Excimer Formation in Highly Luminescent N⁺C⁻N-Coordinated Platinum(II) Complexes. *Inorg. Chem.* **2005**, *44*, 9690–9703. [CrossRef]
66. Klein, A.; Rausch, B.; Kaiser, A.; Vogt, N.; Krest, A. The cyclometalated nickel complex [(Phbpy)NiBr] (Phbpy⁻ = 2,2'-bipyridine-6-phen-2-yl)—Synthesis, spectroscopic and electrochemical studies. *J. Organomet. Chem.* **2014**, *774*, 86–93. [CrossRef]
67. Sandleben, A.; Vogt, V.; Hörner, G.; Klein, A. Redox Series of Cyclometalated Nickel Complexes [Ni((R)Ph(R')bpy)Br]^{+0/-/-2-} (H-(R)Ph(R')bpy = Substituted 6-Phenyl-2,2'-bipyridine). *Organometallics* **2018**, *37*, 3332–3341. [CrossRef]
68. Jensen, K.P. Bioinorganic Chemistry Modeled with the TpSSh Density Functional. *Inorg. Chem.* **2008**, *47*, 10357–10365. [CrossRef] [PubMed]
69. Alrefai, R.; Hörner, G.; Schubert, H.; Berkefeld, A. Broadly versus Barely Variable Complex Chromophores of Planar Nickel(II) from κ^3 -N,N',C and κ^3 -N,N',O Donor Platforms. *Organometallics* **2021**, *40*, 1163–1177. [CrossRef]
70. Vogt, N.; Sandleben, A.; Kletsch, L.; Schäfer, S.; Chin, M.T.; Vicio, D.A.; Hörner, G.; Klein, A. On the Role of the X Coligands in Cyclometalated [Ni(Phbpy)X] Complexes (HPhbpy = 6-phenyl-2,2'-bipyridine). *Organometallics* **2021**, *40*, 1776–1785. [CrossRef]
71. Von der Stück, R.; Schmitz, S.; Klein, A. C-X vs. C-H activation for the synthesis of the cyclometalated complexes [Pd(YPhbpy)X] (HPhbpy = 6-phenyl-2,2'-bipyridine; X/Y = (pseudo)halides). *Inorg. Chem. Res.* **2021**, *5*, 173–192.
72. Lai, S.-W.; Chan, M.C.-W.; Cheung, T.-C.; Peng, S.-M.; Che, C.-M. Probing d⁸-d⁸ Interactions in Luminescent Mono- and Binuclear Cyclometalated Platinum(II) Complexes of 6-Phenyl-2,2'-bipyridines. *Inorg. Chem.* **1999**, *38*, 4046–4055. [CrossRef]
73. Kaim, W.; Fiedler, J. Spectroelectrochemistry: The best of two worlds. *Chem. Soc. Rev.* **2009**, *38*, 3373–3382. [CrossRef]
74. APEX3—Software Suite for Crystallographic Programs; Bruker AXS, Inc.: Madison, WI, USA, 2015.
75. Sheldrick, G.M. Crystal Structure Refinement with SHELXL. *Acta Crystallogr. Sect. C Struct. Chem.* **2015**, *71*, 3–8. [CrossRef]
76. Sheldrick, G.M. A short history of SHELX. *Acta Crystallogr. Sect. A Found. Crystallogr.* **2008**, *64*, 112–122. [CrossRef] [PubMed]
77. Neese, F. The ORCA program system. *Wiley Interdiscip. Rev. Comput. Mol. Sci.* **2012**, *2*, 73–78. [CrossRef]
78. Neese, F. Software update: The ORCA program system, version 4.0. *Wiley Interdiscip. Rev. Comput. Mol. Sci.* **2018**, *8*, 1327. [CrossRef]
79. Chemcraft—Graphical Software for Visualization of Quantum Chemistry Computations. Available online: <https://www.chemcraftprog.com> (accessed on 19 August 2021).
80. Becke, A.D. Density-functional exchange-energy approximation with correct asymptotic behavior. *Phys. Rev. A* **1988**, *38*, 3098–3100. [CrossRef]
81. Perdew, J.P.; Yue, W. Accurate and simple density functional for the electronic exchange energy: Generalized gradient approximation. *Phys. Rev. B* **1986**, *33*, 8800–8802. [CrossRef]
82. Weigend, F.; Ahlrichs, R. Balanced basis sets of split valence, triple zeta valence and quadruple zeta valence quality for H to Rn: Design and assessment of accuracy. *Phys. Chem. Chem. Phys.* **2005**, *7*, 3297–3305. [CrossRef]
83. Grimme, S.; Antony, J.; Ehrlich, S.; Krieg, H. A consistent and accurate ab initio parametrization of density functional dispersion correction (DFT-D) for the 94 elements H-Pu. *J. Chem. Phys.* **2010**, *132*, 154104. [CrossRef] [PubMed]
84. Grimme, S.; Ehrlich, S.; Goerigk, L. Effect of the damping function in dispersion corrected density functional theory. *J. Comput. Chem.* **2011**, *32*, 1456–1465. [CrossRef]
85. Klamt, A.; Schüürmann, G. COSMO: A new approach to dielectric screening in solvents with explicit expressions for the screening energy and its gradient. *J. Chem. Soc. Perkin Trans. 2* **1993**, 799–805. [CrossRef]

-
86. Andrae, D.; Häußermann, U.; Dolg, M.; Stoll, H.; Preuss, H. Energy-adjusted ab initio pseudopotentials for the second and third row transition elements. *Theor. Chim. Acta* **1990**, *77*, 123–141. [[CrossRef](#)]
 87. Petrenko, T.; Kossmann, S.; Neese, F. Efficient time-dependent density functional theory approximations for hybrid density functionals: Analytical gradients and parallelization. *J. Chem. Phys.* **2011**, *134*, 054116. [[CrossRef](#)] [[PubMed](#)]
 88. Hirata, S.; Head-Gordon, M. Time-dependent density functional theory within the Tamm-Dancoff approximation. *Chem. Phys. Lett.* **1999**, *314*, 291–299. [[CrossRef](#)]
 89. Tao, J.; Perdew, J.P.; Stavoverov, V.N.; Scuseria, G.E. Climbing the density functional ladder: Nonempirical meta-generalized gradient approximation designed for molecules and solids. *Phys. Rev. Lett.* **2003**, *91*, 146401. [[CrossRef](#)] [[PubMed](#)]